Phenotyping cardiometabolic disease with magnetic resonance techniques

Paiman, E.H.M.

CHAPTER

When should we use contrast material in cardiac MRI?

Paiman EHM, Lamb HJ

J Magn Reson Imaging. 2017 Dec;46(6):1551-1572. doi: 10.1002/jmri.25754.
Epub 2017 May 8. Review.

ABSTRACT

At present, most of the cardiac magnetic resonance imaging (MRI) examinations rely on contrast-enhanced protocols, but noncontrast alternatives are emerging. Late gadolinium enhancement (LGE) imaging for the detection of myocardial scar can be considered the main cause for the embedding of cardiac MRI into the clinical routine. The novel noncontrast technique of native T1 mapping shows promise for tissue characterization in ischemic and nonischemic cardiomyopathy and may provide additional information over conventional LGE imaging. Technical issues, including measurements variability, still need to be resolved to facilitate a wide clinical application. Ischemia detection can be performed with contrast-based stress perfusion and contrast-free stress wall motion imaging. For coronary magnetic resonance angiography (MRA), protocols with and without contrast material have been developed. Research on coronary atherosclerotic plaque characterization has introduced new applications of contrast material. For MRA of the aorta, which traditionally relied on contrast administration, several noncontrast protocols have become available. This review provides an overview of when to use contrast material in cardiac and cardiac-related vascular MRI, summarizes the major imaging building blocks, and describes the diagnostic value of the available contrast-enhanced and noncontrast techniques. Contrast material in cardiac MRI should be used for LGE imaging for tissue characterization in ischemic or nonischemic cardiomyopathy and may be used for stress perfusion imaging for the detection of ischemia. In cardiac-related vascular MRI, use of contrast material should be avoided, unless high-quality angiography is required that cannot be obtained with noncontrast protocols.

Cardiac magnetic resonance imaging (MRI) has taken an important role in the work-up of cardiovascular disease. Compared to general radiology, MR contrast material is used in a high number of examinations (92%) (1). In this review, we aim to provide an overview of contrast-enhanced and noncontrast cardiac and cardiac-related vascular MRI protocols (**Table 1**). First, the considerations of when to use contrast material in cardiac MRI are discussed. Second, the major imaging building blocks are described, including cine and flow imaging, late gadolinium enhancement (LGE), stress and rest first-pass perfusion and wall motion imaging, native T1 and extracellular volume (ECV) mapping, and magnetic resonance angiography (MRA) of the coronary arteries and large vessels with and without contrast material. Third, most common clinical indications are listed, including myocardial infarction and ischemia, nonischemic cardiomyopathy, cardiac mass, and visualization of the coronary arteries and large vessels, with an overview of the diagnostic value of the available contrast-enhanced and noncontrast techniques.

CONTRAST MATERIAL IN CARDIAC MRI

Safety

REGULATION. The decision whether gadolinium-based contrast agents can be safely used in cardiac MRI is dependent on the individual patient characteristics, similar to general radiology. In patients with previous severe hypersensitivity reactions, contrast material should be avoided. For contrast administration in patients with impaired renal function, pregnancy or lactation, institutional, regional, or national guidelines should be followed (2-5). If noncontrast techniques with comparable diagnostic performance are available, those should be preferred over contrast-enhanced techniques. If contrast administration is indicated, the administered dosage should be as low as possible.

It should be noted that administration of gadolinium-based contrast material in cardiac and cardiac-related vascular MRI is not regulatory-approved (6). The decision to use gadolinium chelates in cardiac MRI should be based on strong evidence in the literature and the prescribing clinician is responsible for maintaining records of the contrast agent's use and effects (7). The decision whether or not to discuss the off-label status of a product with the patient is rather an ethical than a legal issue, and should be based on professional judgment (8). In our center, similar to any other medical intervention, we inform the patient in advance that there is a risk of adverse events and tailor more detailed information to the individual patient. Given the widely accepted use of gadolinium-based contrast material in cardiac MRI, we do not specifically address the off-label status. Up-to-date figures regarding informed consent procedures among centers are not available.

Table 1. Clinical protocols for contrast-enhanced and noncontrast cardiac and cardiac-related vascular MRI.

Indication	MRI protocol with contrast material	MRI protocol without contrast material
Myocardial infarction (viability assessment, postreperfusion therapy)	LGE imaging ECV mapping	Native T1 mapping
Myocardial ischemia (viability assessment, postreperfusion therapy)	Stress perfusion imaging	Stress wall motion imaging
Nonischemic cardiomyopathy (including arrhythmia and myocarditis)	LGE imaging ECV mapping Early gadolinium enhancement (for myocarditis)	Native T1 mapping T2-weighted black and bright blood imaging (not discussed) T2 and T2* mapping (not discussed)
Cardiac mass	First pass imaging Post contrast T1-weighted imaging LGE imaging	T1-and T2-weighted imaging (with and without fat suppression) Native T1 and T2 mapping
Coronary artery anomalies/ patency	Contrast-enhanced T1-weighted MRA	Time-of-flight imaging Balanced SSFP imaging
Large vessels (including congenital disease and pulmonary vein evaluation pre- and postablation)	Contrast-enhanced T1-weighted MRA (also for pulmonary vein evaluation)	Balanced SSFP imaging (thoracic aorta) Partial-Fourier FSE imaging (peripheral arteries) Time-of-flight imaging Phase-contrast imaging Quiescent-interval slice selective (QISS) imaging

For details regarding standardized protocols and contrast dosing, see the standardized cardiac MR protocols of the Society for Cardiovascular Magnetic Resonance (SCMR) (24). LGE: late gadolinium enhancement; ECV: extracellular volume; MRA: magnetic resonance angiography; SSFP: steady-state free precession; FSE: fast spin echo.

HYPERSENSITIVITY REACTIONS. Based on the reported numbers in routine cardiac MRI, use of gadolinium chelates in a clinical cardiac MRI setting can be considered safe in terms of frequency and severity of adverse reactions. Retrospective analysis, based on 158,796 MR exams in the United States, showed an event rate of 0.055% for cardiac MRI, compared to 0.059% for overall MRI (9). The EuroCMR Registry, including 37,788 patients in 57 European centers, reports a number of 0.12%, with most of the adverse events being mild (eg, rashes and hives, nausea, or flushes) (10). No deaths due to contrast administration in cardiac MRI were reported. The above number is comparable to data on adverse events in general radiology, ranging from 0.059% to 0.3% in recent reports (9,11,12).

NEPHROGENIC SYSTEMIC FIBROSIS. The first report on nephrogenic systemic fibrosis (NSF), observed in patients with endstage chronic kidney disease, was published in 2000 (13). As studies found an association between high dosage of gadolinium chelates (0.2–0.3 mmol/kg) and increased incidence of NSF, double or triple dosing is no longer common practice (14,15). Although the association between NSF and gadolinium chelates in patients with renal failure is well recognized, the mechanism and the relation to the different compounds is still controversial. Prevailing hypothesis explaining the differences in the number of reported cases is the difference in gadolinium chelate stability. Several reviews are available regarding the association between gadolinium chelates and NSF (14-16).

GADOLINIUM DEPOSITION IN THE BRAIN. In 2014 the first report was published that showed that serial injection of gadolinium-based contrast material correlated with a signal intensity increase in the dentate nucleus and the globus pallidus on T1-weighted MRI, also in patients with normal renal function (17). Subsequent studies found evidence of gadolinium deposition in the brain of deceased patients and a correlation between the cumulative intravenous dose and the total amount of gadolinium stored in the tissue (18,19). Comparable to NSF, it is hypothesized that the potential of gadolinium-based contrast agents to cause hyperintensities or gadolinium deposition in the brain is related to stability. In the last 2 years, multiple retrospective patient studies and prospective animal studies have been performed, as summarized in the review of Radbruch (20). Up until now, the clinical relevance of the gadolinium brain deposition is unknown. It has not been associated with neurologic or biological adverse effects. A definite conclusion has not been formed yet and multiple research groups are currently working on this topic.

SPECIFIC POPULATIONS. As impaired renal function increases the risk of NSF, use of gadolinium chelates in patients with renal dysfunction should be avoided unless the diagnostic information is absolutely required and cannot be obtained with noncontrast MRI or other modalities. The risk of NSF is highest in patients with chronic severe kidney disease (glomerular filtration rate [GFR] <30 ml/min/1.73 m^2) or acute kidney injury (21). For all patients at risk of chronically reduced renal function (including age >60 years, hypertension, or diabetes), GFR should be estimated through laboratory sampling. Relatively unstable, high-risk gadolinium-based contrast agents (ie, gadopentetate dimeglumine, gadodiamide, and gadoversetamide) should be avoided. The remaining gadolinium-based contrast agents should be used with caution. In patients with endstage renal disease, contrast administration should be followed by dialysis (2-5,22). There are limited studies on the safety of contrast administration in pregnant or nursing women. Only if the potential benefits justify the potential risk, gadolinium-based contrast material may be used (2-5,22). Several gadolinium chelates are approved for pediatric use (2–18 years) (2).

Dosage

Approved clinical doses range from 0.1 and 0.3 mmol/kg body weight, although for most labeled indications the recommended dose is 0.1 mmol/kg. Contrast dose as used in cardiac MRI practice is in general higher than the recommended label dose. A meta-analysis on the administered dose of gadolinium-based contrast material in cardiac MRI trials found a median total dose per exam (LGE imaging and/or perfusion testing) of 0.2 mmol/kg (23). The document on standardized cardiac MR protocols of the Society for Cardiovascular Magnetic Resonance (SCMR) provides a practical overview of the recommended contrast and chasing bolus doses and injections rates (0.05–0.1 mmol/kg for perfusion imaging and 0.1–0.2 mmol/kg for LGE imaging) (24).

There is limited evidence on the efficacy of infarct detection by LGE in relation to dosage. To date, there is one multicenter, double-blinded, randomized trial, which studied the diagnostic performance of LGE in patients with acute and chronic myocardial infarction, for varying gadoversetamide doses. Sensitivity and specificity for detection of myocardial infarction increased with increasing doses of 0.1, 0.2, and 0.3 mmol/kg (for acute infarction 84, 95, 99%, respectively, and for chronic infarction 83, 87, 94%, respectively) (25). For perfusion cardiac MRI, there are two dose ranging multicenter trials that used gadopentetate dimeglumine.26,27 For a dosage of 0.05, 0.10, or 0.15 mmol/kg for rest and stress perfusion imaging (total dose per exam 0.1, 0.2, and 0.3 mmol/kg), Wolff et al (26) reported an area under the receiver-operating curve (AUC) of 0.90, 0.72, and 0.83, respectively, for the detection of obstructive coronary artery disease, compared to quantitative coronary angiography. Giang et al (27) reported an AUC of 0.53, 0.91, and 0.86, respectively. Although higher doses were shown to result in increased myocardial enhancement, higher doses did not result in improved diagnostic performance, as susceptibility artifacts may have led to false-positive findings.

Types of contrast agents

CHEMICAL STABILITY. The chemical structure of gadolinium chelates can be categorized as ionic versus nonionic and linear versus macrocyclic compounds. Gadolinium chelates need to be highly stable, to prevent release of free Gd^{3+} and guarantee safety. Stability is defined by the thermodynamic and kinetic stability constants and the chelates metal selectivity for Gd^{3+} over another metal species. Thermodynamic stability refers to the energy difference between the Gd^{3+} ligand complex before and after chelation and can be explained as "how tightly the ligand binds with Gd^{3+}." Kinetic stability is a measure of the activation energy needed to change the state of the Gd^{3+} complex and can be interpreted as "how easily Gd^{3+} is released from the chelate" (28). In general, ionic (negatively charged) chelates have higher stability compared to nonionic (uncharged) chelates, and a macrocyclic is favorable in terms of stability compared to a linear structure (29).

RELAXIVITY. Most gadolinium chelates have comparable T1 and T2 relaxivity (relaxation rate as a function of contrast agent concentration), except for gadofosveset trisodium, gadoxetate disodium, gadobenate dimeglumine, and gadobutrol, which have increased relaxivity compared to other agents. As gadobutrol is available in high concentration (1.0 mol/L), in combination with its high relaxivity, gadobutrol provides the largest T1 shortening effects per volume (30). In LGE imaging, gadobutrol results in superior contrast between infarct and blood, but generates similar contrast between infarct and normal tissue, compared to gadobenate dimeglumine (31).

NONBLOOD POOL VERSUS BLOOD POOL. All gadolinium chelates are extracellular (nonblood pool) agents, except for gadofosveset trisodium. Gadofosveset is an albumin-binding (blood pool) agent with longer plasma half-lives. For aorta MRA, when using gadofosveset, smaller total amounts are required and the imaging window is prolonged for up to 30–60 minutes after contrast administration (32). Improved image quality was shown for coronary MRA when using gadofosveset compared to gadobenate dimeglumine (33). However, as intravascular contrast agents do not allow for LGE imaging, gadofosveset cannot be used in a comprehensive protocol for the evaluation of both coronary artery patency and scar tissue. Currently, gadofosveset is commercially not available.

FERUMOXYTOL. Ferumoxytol has been proposed as an alternative to gadolinium-based contrast material. Ferumoxytol is an ultrasmall superparamagnetic iron oxide particle (USPIO), approved for the treatment of iron-deficiency anemia in patients with chronic kidney disease (34). In some institutions, it is used in standard clinical examinations including aorta, coronary, and peripheral vascular imaging (35). In contrast to MRA, the experience with ferumoxytol for myocardial tissue imaging is limited.

Ferumoxytol can be prescribed in patients with reduced renal function. Another advantage is its prolonged intravascular half-life of more than 15 hours. Timing of acquisition relative to contrast administration is not needed and prolonged or repeated imaging is possible (36). One concern, however, is the rare, but serious, hypersensitivity reactions that are observed in the context of the therapeutic use of ferumoxytol in dialysis centers (37). For imaging applications, in contrast, ferumoxytol is used at a much lower dose. To date, there are few studies on the safety of ferumoxytol as a contrast agent in MRI (38).

MAJOR BUILDING BLOCKS OF CARDIAC MRI

Cine imaging

Each clinical cardiac MR examination starts with cine long-axis (2-chamber, 4-chamber, and 3-chamber view) and short-axis images for the assessment of left ventricular (LV) function and structure. Recommended method is balanced steady-state free precession (SSFP) (24). Balanced SSFP employs the high T2/ T1 ratio of blood compared to myocardium to generate a high signal-to-noise ratio (SNR) and high contrast to noise ratio (CNR), without the need of contrast administration (39).

Flow imaging

Velocity of flow across valves or in vessels can be quantified using phase-contrast techniques. Conventionally, a motion-encoded gradient in one direction is applied to quantify through-plane flow (2D flow) (24). For more detailed flow information, velocity-encoding in three directions is possible (4D flow) (40). Flow imaging does not require contrast administration.

Late gadolinium enhancement

LGE imaging for the visualization of myocardial infarction has been an important and pioneering development in cardiac MRI. As explained by Kim et al (41), in myocardial infarction the functional capillary density is diminished, as a result of microvascular damage in combination with an increased distribution volume caused by, for example, edema and necrosis (acute stages) and replacement scar tissue (chronic infarction). A decrease in functional capillary density causes prolonged wash-in/wash-out time constants of the contrast agent, because of the decrease in capillary surface area available for solute transport and the increase in diffusion distance in the interstitium to fill the extracellular space. As the T1 relaxation time increases with the wash-out of contrast agent, healthy myocardium appears relatively hypoenhanced, compared to the delayed hyperenhancement in infarcted myocardium.

The technique of LGE for myocardium infarct imaging has been improved since the introduction of phase-sensitive inversion recovery (PSIR) imaging, compared to the conventional magnitude-reconstructed technique (42,43). Whereas in magnitude reconstruction, the rendered image intensity relies on the magnitude of the net magnetization, in phase-sensitive techniques, it depends on the polarity additionally. The PSIR technique prevents diminished contrast when the inversion time (TI) is earlier than the null time for healthy tissue, with therefore less variation in apparent infarct size (44). Other advances include free-breathing techniques; for example, respiratory navigator gated high-resolution whole-heart 3D LGE (**Figure 1**) (45). High-resolution whole-heart LGE facilitates scar detection for the complete LV, with precise scar delineation. Another free-breathing approach is automatic, nonrigid registration for motion correction. This approach enables robust LGE imaging, with high image quality and diagnostic performance, without the patient needing to perform breath-holds (46).

Since the introduction of modified Look-Locker inversion recovery (MOLLI)-based T1 mapping, not only fast and reliable pixel-wise T1 mapping became possible, but also synthetic inversion recovery (IR) images could be generated. Synthetic IR images can be calculated retrospectively at any TI, based on the myocardial T1 values generated with a MOLLI acquisition. Conventional LGE acquisition could then be eliminated, if T1 mapping is already in the clinical protocol (47).

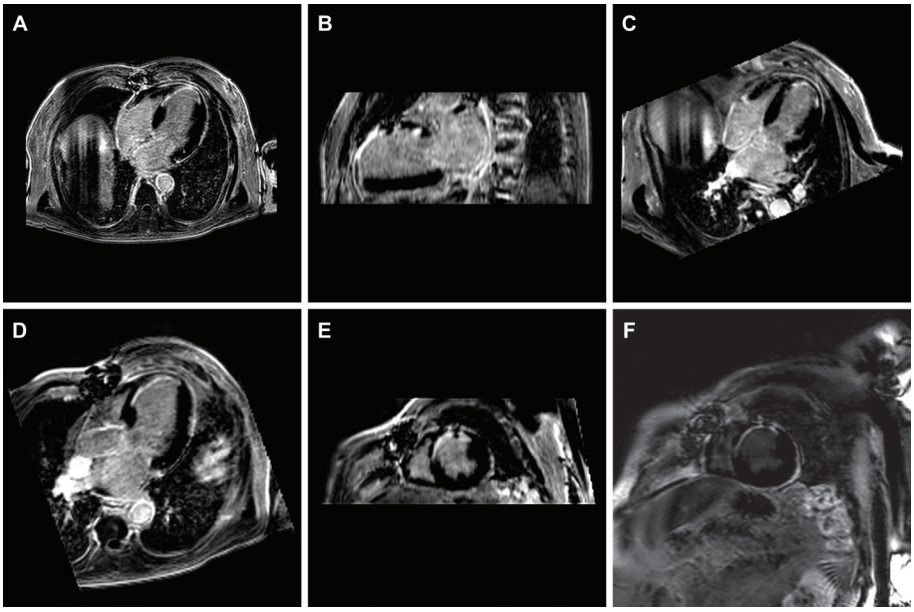

Figure 1. Example of respiratory navigator gated high-resolution whole-heart 3D late gadolinium enhancement (LGE) imaging: a 77-year-old man, with a history of anteroseptal myocardial infarction, multiple coronary artery bypass grafts, and percutaneous coronary intervention. (**A**) Transverse stack covering the complete left ventricle. Given the high spatial resolution, multiplanar reformatting can be performed with high in-plane resolution: reformatted 2-chamber (**B**), 4-chamber (**C**) 3-chamber (**D**), and short-axis (**E**) view. (**F**) For comparison, the conventional 2D LGE short-axis image is provided.

Stress perfusion and stress wall motion imaging

Stress and rest first-pass perfusion provides insight into both reversible and irreversible myocardial ischemia, and can be used to test for viability in chronic ischemic heart disease or to verify successful revascularization. At rest, a lesion is flow-limiting not until a luminal narrowing of >85% (48), since stenotic coronary arteries can restore flow by vasodilation. During pharmacological stress, however, stenotic coronary arteries cannot increase flow to meet the increasing myocardial demands. Based on relative perfusion deficits, stress perfusion is able to detect a stenosis of >50% (49).

First-pass perfusion imaging measures the first pass of a contrast bolus through the ventricular cavity and myocardial tissue, based on T1-weighted dynamic imaging (**Figure 2**)

(50). The signal intensity correlates with the amount of contrast material, which allows both qualitative and (semi)quantitative analysis of perfusion and hypoperfusion. The initial part of the signal intensity curve can be quantitatively analyzed, avoiding fast redistribution of contrast material into the extracellular space (51).

A contrast-free alternative to stress perfusion cardiac MRI is stress wall motion imaging, which allows detection of ischemia by qualitative evaluation of regional wall motion during infusion of increasing doses of pharmacological stress agents (52). In general, adenosine (a vasodilator) is used for the detection of stress-inducible perfusion deficits, and dobutamine (a positive inotropic and positive chronotropic) for wall motion abnormalities (53).

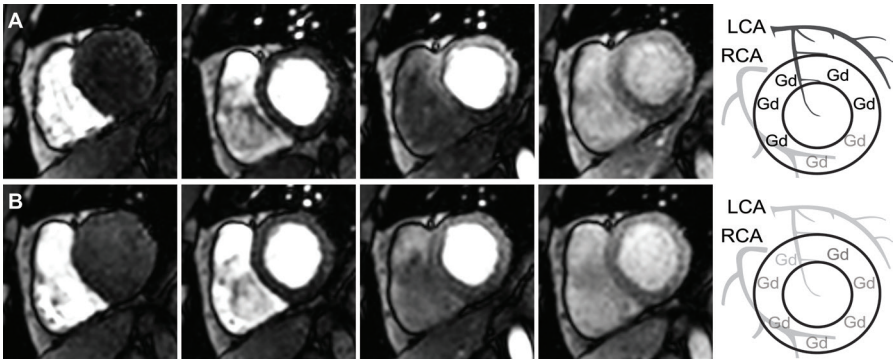

Figure 2. Example of first-pass adenosine stress and rest perfusion cardiac MRI: a 57-year-old man with a significant perfusion deficit in the inferior segments. (**A**) Dynamic adenosine stress perfusion MR images (dosage of gadoterate meglumine [Dotarem]: 0.1 mmol/kg). In contrast to the left coronary artery (LCA), the stenotic right coronary artery (RCA) cannot further dilate in response to stress, which results in pronounced hypoenhancement of the inferior segments. (**B**) Dynamic rest perfusion MR images (dosage of gadoterate meglu-mine [Dotarem]: 0.1 mmol/kg). The differences in perfusion between the inferior segments and the other segments are less pronounced. The impaired blood flow in the stenotic RCA during stress is largely restored by vasodilation in rest.

Native T1 and extracellular volume mapping

Advances in cardiac MRI have rendered it feasible to not merely obtain cardiac T1-weighted images, but to estimate the T1 relaxation times quantitatively, and display them pixel-wise. The concept of T1 mapping is sampling the recovery of magnetization after saturation or inversion and fitting a T1 recovery curve. T1 maps can be acquired solely without contrast material (native T1), or both prior and after contrast agent administration (postcontrast T1), which enables calculation of ECV maps (**Figures 3 and 4**).

With the technique of ECV mapping, the myocardium is dichotomized into an intracellular compartment (myocytes) and extracellular compartment (extracellular matrix and vessels) (54). The difference in T1 relaxation rate (1/T1) of blood between pre-and postcontrast imaging

is converted with the hematocrit value into a reference for plasma T1. Based on T1 changes in myocardial tissue, the ratio of extracellular to myocardial volume can be calculated. Whereas native T1 values are a reflection of both intra-and extracellular characteristics, ECV can be seen as an estimate of the extracellular space, which is affected by edema, fibrosis, or amyloid, etc.

A drawback of ECV mapping is the dependence on several measurements, including native and postcontrast T1 images, blood T1, and hematocrit. All need to be measured correctly to avoid an accumulation of errors. To facilitate implementation of ECV mapping, there have been methods suggested for ECV estimation without blood sampling to determine the hematocrit level (55). The relationship between hematocrit and the T1 relaxation rate of blood can be calibrated, which is used to generate a synthetic ECV. Treibel et al (55) found a linear relationship between the native T1 relaxation rate of blood and hematocrit. Synthetic ECV values based on this relationship correlated well with conventional ECV and histology.

There are several limitations that hamper translation of native T1 mapping and ECV mapping from research to clinical setting. Measured T1 values vary with vendor and field strength (higher at 3T compared to 1.5T), type of pulse sequence (most applied is the MOLLI sequence), and across the myocardium (higher in septal than lateral wall) (56). The ECV mapping technique, in which systematic differences are cancelled out, may be more comparable across MR field strengths, acquisition protocols, and imaging centers. For clinical application, T1 mapping should be highly reproducible to avoid misclassification of patients (insufficient precision, more than inaccuracy, is a major limitation for clinical use) (57). Certain technical development is needed to reduce measurement variability, to enable the detection of differences between disease groups, diagnosis in the individual patient, or monitoring of therapy effect (58).

In the SCMR expert consensus document on T1 and ECV mapping, recommendations regarding site preparation, scan protocols, and quality control are listed (59). Tight control of the scan protocol is required, as it is not fully known to what extent changes in software updates or imaging parameters affect T1 mapping. New T1 mapping sequences should be validated in phantoms with T1 values in the range of the expected values and with simulation of a range of heart rates. Ideally, for each particular setting, normal values should be acquired in a healthy control group. In multicenter studies, stratified analysis is recommended, to account for variations among centers. Recently, the first steps towards multicenter-based reference values have been made, registries are in progress (SCMR Registry, HCM Registry, UK Biobank), quality control systems are explored, and commercial sequences are available.

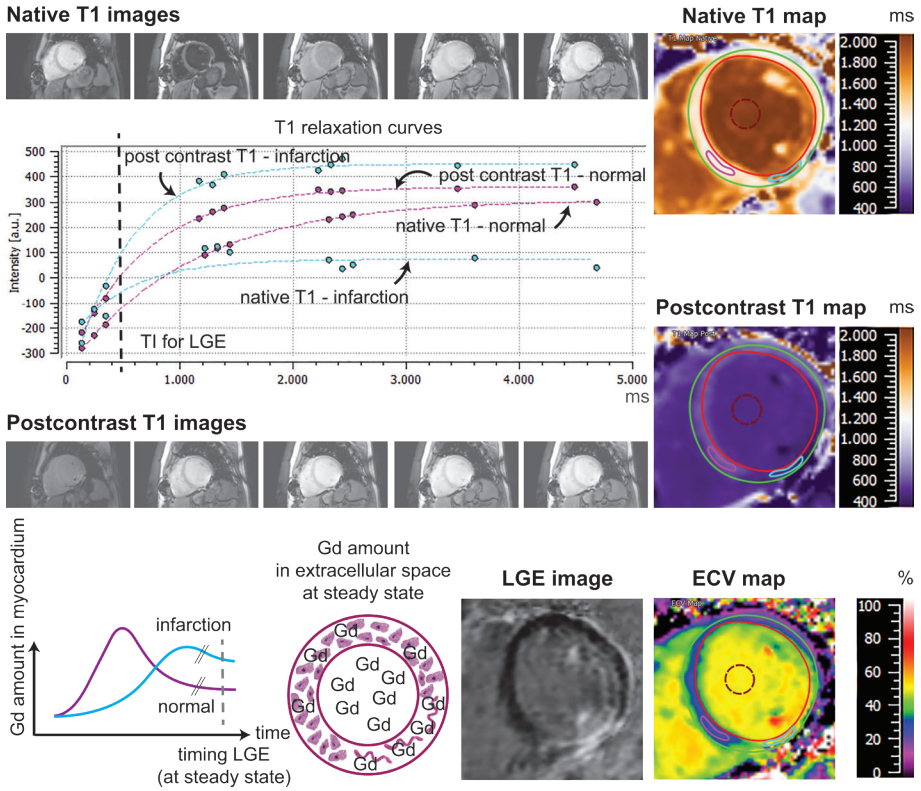

Figure 3. Concept of native and postcontrast T1 mapping and late gadolinium enhancement (LGE) imaging. A 54-year-old man, with an inferolateral myocardial infarction and prior sternotomy. (***Upper panel***) T1 mapping is performed before and after contrast adminis-tration. Presented T1 relaxation curves represent the areas with normal (purple) and infarcted (blue) myocardium. T1 mapping is based on the 3(3)3(3)5 modified Look-Locker (MOLLI) sequence. The T1 relaxation curve is sampled after three 1808 inversion pulses, with a rest period of 3 heart beats (respectively 3, 3, and 5 images at diastole are obtained). Based on the 11 images, the T1 relaxation curve can be fitted pixel-wise. (***Lower panel***) 10–15 minutes after contrast administration, a dynamic steady state in gadolinium (Gd) concen-tration between myocardium and blood pool is established. Given the increased extracellular volume (ECV) of infarcted myocardium, due to necrosis and/or replacement fibrosis, the amount of Gd is higher in infarcted compared to normal myocardium at steady state, which results in increased T1 shortening. In late gadolinium enhancement (LGE) imaging, the inversion time (TI) nulls normal myocar-dium. Based on native and postcontrast T1 maps, the ECV map can be calculated. Note: T1 relaxation times vary with vendor, field strength, and pulse sequence. (Image analysis in Medis Suite 2.1.)

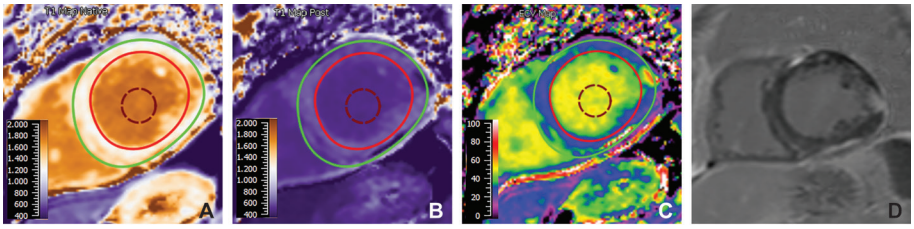

Figure 4. Example of native T1 mapping (**A**), postcontrast T1 mapping (**B**), extracellular volume (ECV) mapping (**C**), and LGE imaging (**D**): a 65-year-old man, scheduled for reablation of atrial fibrillation. The patchy areas of increased ECV correspond to the areas of LGE. Cardiac MRI findings are suggestive of nonischemic cardiomyopathy, myocarditis, sarcoidosis, or storage disease. (Image analysis in Medis Suite 2.1.)

Coronary MRA with and without contrast material

In contrast-based coronary MRA, contrast between blood and surrounding tissue is the result of the T1 shortening effect of contrast material. In general, extracellular gadolinium chelates are used that extravasate in about 10 to 15 minutes after administration. Hence, contrast-enhanced coronary MRA is limited by the fast redistribution of the contrast agent, which reduces the SNR for the coronary arteries and increases the signal in the coronary veins. Proposed techniques to obtain a prolonged blood signal enhancement time is slow infusion (0.3 ml/s) of contrast media (61,62), or using albumin-binding contrast agents with longer plasma half-lives (63).

A commonly used technique for coronary MRA without contrast material is balanced SSFP (64). At 3T, balanced SSFP is more challenging, due to the sensitivity to magnetic field inhomogeneities and increased energy deposition with increasing field strength. Therefore, 3T coronary MRA generally relies on gradient echo (GRE) sequences, in which contrast is generated using time-of-flight techniques (61). Noncontrast coronary MRA can be combined with T2 preparation for suppression of myocardium and deoxygenized venous blood and fat saturation for nulling of epicardial fat. An alternative technique for improved contrast between coronary vessels and myocardium is magnetization transfer (65). The magnetization transfer pulse saturates myocardium via transfer of magnetization between water and macromolecular protons. Magnetization transfer has potential for the visualization of the coronary veins, as the magnetization transfer pulse leaves venous blood unaffected, which is an advantage as compared to T2 preparation. A recently introduced contrast-free technique for coronary MRA is Dixon-based (**Figures 5 and 6**), which has more consistent and reliable fat suppression as compared to fat-saturated balanced SSFP (66).

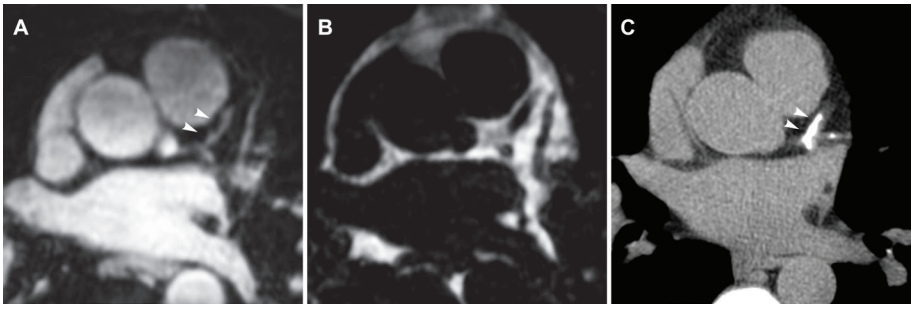

Figure 5. Example of respiratory navigator-gated 3D whole-heart coronary dual-echo Dixon gradient echo (GRE) imaging with water-fat separation: a 57-year-old man with familial hypercholesterolemia and a positive family history for coronary artery disease. (**A**) Transverse Dixon water-image. (**B**) Transverse Dixon fat-image. (**C**) CT image for calcium scoring. Note the severe calcification (arrows) in the left main (LM) coronary artery and proximal left anterior descending (LAD) and left circumflex coronary artery, corresponding to the dark areas on the water-fat resolved Dixon coronary MRA images (arrows).

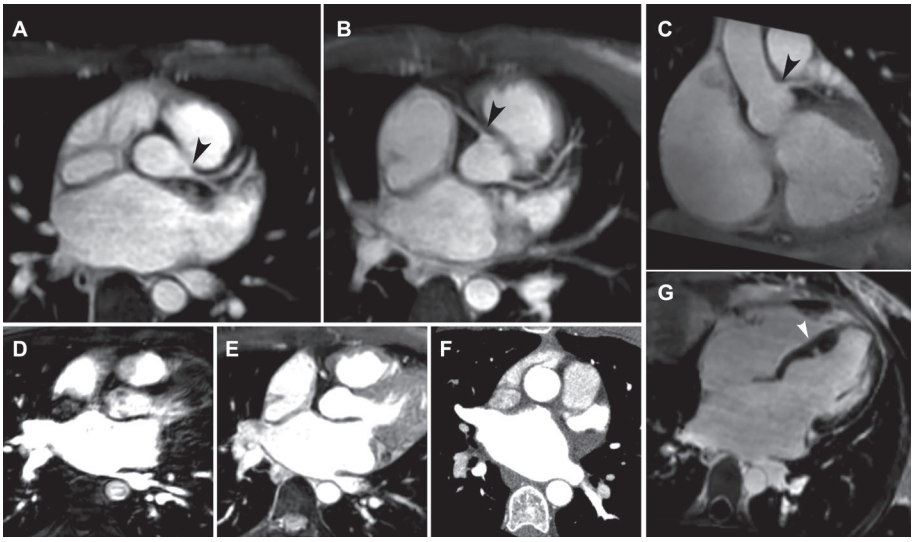

Figure 6. Example of a comprehensive cardiac MR examination prior to catheter ablation for atrial fibrillation: a 38-year-old woman, scheduled for reablation. (**A–C**) Reformatted transverse (A,B) and coronal (C) Dixon water-images for the identification of the left main (LM) coronary artery, which serves as an anatomic landmark for the integration of the MR images with the electro-anatomical maps. Note the origo of the left and right coronary arteries (black arrows). (**D**) Contrast-enhanced MRA of the pulmonary veins for the evaluation for anatomic variants. In this patient, the left upper and lower lobe pulmonary veins have one common ostium into the left atrium, while the right pulmonary veins drain into separate ostia. The presented image shows the left common ostium and the right upper ostium. (**E**) Noncontrast-enhanced Dixon water-image of the ostia of the pulmonary veins. (**F**) For comparison, the contrast-enhanced CT image of the ostia of the pulmonary veins is provided. (**G**) Reformatted 4-chamber late gadolinium enhancement (LGE) for the evaluation of myocardial scar. Note the midventricular septal hypertrophy with a deep myocardial crypt (white arrow).

Coronary vessel wall imaging and plaque characterization

In the research setting, more advanced coronary MRA techniques are explored, including techniques for coronary vessel wall imaging and plaque characterization. The coronary vessel wall can be visualized using nonenhanced, black-blood techniques. Double-IR nulls the signal of flowing blood, rendering a bright vessel wall; the addition of fat suppression improves contrast between outer vessel wall and epicardium (67,68). Measurement of the thickness of the coronary vessel wall may have potential for the detection of subclinical atherosclerosis (69,70).

Vessel wall remodeling and inflammation may be visualized with use of contrast-enhanced techniques. In the carotid arteries, the rate of contrast enhancement on dynamic MRI highly correlates with histological evidence of plaque angiogenesis and macrophage content (71). Also, as confirmed by histologic studies, gadolinium enhancement can discriminate the fibrous cap from the lipid-rich necrotic core, which lacks vasculature and matrix (72). In the coronary arteries, likewise, it has been observed that some plaques express gadolinium uptake, while others do not (73), which may be associated with an expansion of the extracellular volume of the coronary wall as a result of edema or fibrosis, with increased neovascularization and vascular permeability or with endothelial dysfunction. Another study showed that coronary segments with strong delayed gadolinium enhancement resemble the segments with severe atherosclerosis on computed tomography (CT) (74). Others found evidence of increased wall enhancement, probably as a result of inflammatory activity in coronary atherosclerosis, in the acute stage of the acute coronary syndrome, compared to a drop in signal intensity and in extent several months postmyocardial infarction (75). Furthermore, tissue-specific contrast agents have been introduced for detecting disease activity; for instance, USPIO, which is taken up by macrophages within the atherosclerotic plaque (76), fibrin-specific contrast agents for thrombi labeling (77), or elastin-specific contrast agents that detect the increased expression of elastin during plaque development (78).

There are several contrast-free MRI techniques for plaque characterization. Plaque regions can be characterized as fibrocellular, lipid-rich, or calcified, on the basis of biochemical and biophysical parameters, such as chemical composition or molecular motion and diffusion, by using different contrast-weighted techniques (T1-or T2-weighted, proton density, time-of-flight techniques) (79). For instance, coronary thrombus and intraplaque hemorrhage can be identified on noncontrast-enhanced T1-weighted MRI, based on the hyperintense signals as a result of the short T1 relaxation time (80,81).

MRA of the aorta with contrast material

Contrast-enhanced MRA techniques were introduced in the 1990s by Prince (82), to overcome the limitations related to the flow-dependency of noncontrast MRA at that time. The first pass of the contrast bolus through the large arteries is visualized by using a T1-weighted GRE sequence. The short repetition times selectively saturate the surrounding tissue. In contrast, because of the short T1 relaxation time of gadolinium, the blood pool remains unsaturated. The short echo times minimize flow-induced intravoxel dephasing, for example due to turbulent flow in stenosis. A major advantage of contrast-enhanced over noncontrast MRA is the robustness, also when inflow is limited (including slow, retrograde, or turbulent flow), and the short acquisition time, which minimizes motion artifacts and enables breath-holding. Since contrast agent rapidly redistributes into the tissue, additional bolus injections are not that useful. Therefore, an important limitation for spatial coverage and resolution is the short duration of the arterial phase. A pitfall is the timing of the acquisition relative to the timing of the contrast bolus, to ensure a perfect arterial phase without venous enhancement (83). Several methods are recommended for optimized timing: measurement of the time to peak enhancement following injection of a test bolus, based on transaxial images at the level of the distal abdominal aorta; an automated bolus triggering technique; or rapid multi-phase 3D acquisitions without timing (24).

MRA of the aorta without contrast material

Noncontrast MRA sequences can be categorized as inflow-based, flow-encoding, cardiac phase-dependent, or relaxation-based techniques (84-86). First, MRA protocols in the 1980s were noncontrast time-of-fight sequences (inflow-based techniques) (87). Whereas repeated excitation saturates stationary spins, inflowing blood spins with fresh longitudinal magnetization generate high signal intensity. In contrast to vessels with continuous laminar flow, in vessels with slow, retrograde, or turbulent flow blood, spins within the slice become partially saturated. Contamination by high signal of inflowing venous blood can be minimized by presaturation of the upstream venous region. Whereas time-of-flight techniques are still widely used in intracranial angiography, it is less suitable for peripheral arteries (the transverse instead of craniocaudal acquisition prolongs the acquisition time) and thoracic aorta (the complex anatomy makes it prone to in-plane signal loss).

An inflow-based alternative developed in the 1980s is phase-contrast MRA (88). Flowing blood, in contrast to stationary tissue, acquires a substantial phase change as the result of bipolar velocity-encoding gradients. As the signal intensity is proportional to the velocity of flowing blood, phase-contrast MRA can be used to extract additional hemodynamic information (89). Compared to the time-of-flight method, phase-contrast MRA results in superior background suppression. Its clinical use for MRA of the aorta, however, is limited by the relatively long acquisition time and the reduced signal intensity in relation to pulsatile blood flow.

Figure 7. Example of noncontrast-enhanced MRA of the aorta: a 34-year-old man, diagnosed with Marfan's disease. (**A,B**) Reformatted sagittal Dixon fat-image (A) and water-image (B) along the thoracic aorta. (**C**) 3D visualization based on Dixon-water MRA of the aorta. (**D,E**) Conventional black-blood MRA of the aorta. Note the flow artifacts, due to inadequate suppression of in-plane flow (arrows). (**F,G**) Conventional cine balanced steady-state free precession (SSFP) for measurement of the aortic root dimensions.

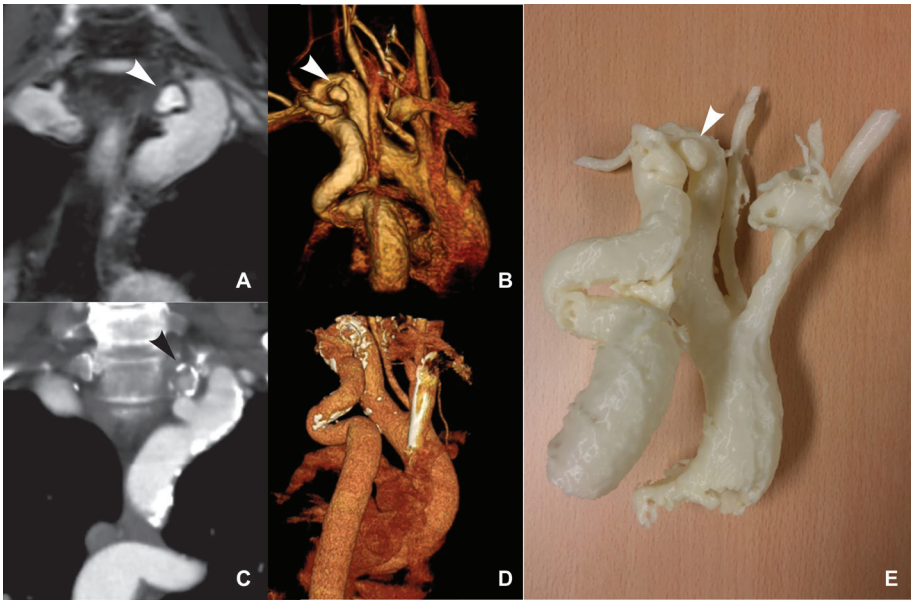

Figure 8. Example of noncontrast-enhanced water-fat resolved Dixon MRA of the thoracic aorta: a 66-year-old man, known with a cervical aortic arch (type C: left cervical arch with right-sided looping descending aorta). (**A,B**) Dixon water-image: (A) enlarged coronal view of the cervical aortic arch and (B) posterior view of the 3D visualization of the aorta. Note the aneurysm at the cervical loop (white arrows) (**C,D**). For comparison, contrast-enhanced CT images are provided: (C) enlarged coronal view. Note the calcified wall of the aneurysm (black arrow); (D) posterior view of the 3D visualization. (**E**) Posterior view of the 3D print, based on Dixon MRA of the aorta.

A novel inflow-based technique is quiescent-interval slice-selective (QISS) MRA, which is a 2D ECG-gated single-or two-shot balanced SSFP acquisition with slice-selective IR preparation for suppression of background tissue (90). Saturation of the image slice is timed at the beginning of the systole, followed by a quiescent inflow period in the systolic phase, with the balanced SSFP acquisition during diastole. Given the relatively long inflow period and the timing during systole, the refreshment effect in QISS is high compared to the conventional time-of-flight technique. As QISS acquires a complete slice per cardiac cycle, QISS has a relatively short acquisition time. The inflow effect is less dependent on blood flow velocity, flow patterns, and heart rate. A drawback of QISS is the dependency on magnetic field homogeneity, as it is a balanced SSFP-based acquisition. A cardiac-phase-dependent technique is ECG-gated 3D partial-Fourier fast spin echo (FSE) (91). Imaging is based on the physiological difference in systolic and diastolic blood flow velocity. Spins are repeatedly refocused during the echo train. Fast-flowing blood in the arterial phase results in loss of signal, whereas slow flow in the diastole causes high signal intensity. Bright-blood MRA is generated by subtraction of the systolic and diastolic acquisition. To reduce the total scan time, commonly one or two shots per slice are

used. T2 blurring is minimized by shortening of the echo train length using a partial-Fourier echo train. ECG-gated 3D partial-Fourier FSE is extensively applied, given the large craniocaudal coverage and the insensitivity to magnetic field inhomogeneities. A drawback for thoracic aortic MRA is the susceptibility to artifacts caused by the multidirectional flow patterns.

Balanced SSFP is a relaxation-based technique. Image contrast relies on the difference in T2/T1 relaxation times between blood and surrounding tissue. Typically, 3D balanced SSFP is combined with an IR preparation pulse. With an appropriate TI, background tissue is nulled, and inflowing blood from outside the IR-prepared volume is visualized with high signal intensity. Balanced SSFP has little dependence on blood flow, which makes it less prone to artifacts. Furthermore, respiratory navigator-gated 3D dual-echo Dixon GRE with water–fat separation, which has been reported in the literature for coronary artery imaging, can be used for the visualization of the aorta as well (**Figures 7 and 8**) (66).

New promising techniques

MYOCARDIAL ARTERIAL SPIN LABELING. Myocardial arterial spin labeling (ASL) has been studied as a contrast-free alternative to first-pass perfusion imaging (92). Arterial spins are magnetically labeled, thereby creating an endogenous tracer. Subtraction of the images with and without prior labeling of inflowing blood results in signal intensities that are proportional to myocardial blood flow. Contrary to first-pass perfusion imaging, which visualizes relative signal intensities across the ventricle, ASL enables absolute quantification of myocardial blood flow. ASL is still challenging and limited to the research domain. Only relatively small signal changes can be achieved with the labeling. Given the pulsatile blood flow, the labeling pulse and image acquisition need to be synchronized to the cardiac cycle. Also, interfering effects of cardiac motion and the multidirectional blood flow complicate adequate selection of the labeling volume.

Myocardial ASL can be performed using flow-sensitive alternating inversion recovery (FAIR), in which labeling and imaging is timed at mid-diastole in consecutive heartbeats, or with the more recent steady-pulsed ASL (spASL) technique, in which the timing is in end-systole and mid-diastole, respectively. Although spASL is more efficient, a drawback is its sensitivity to errors in ECG triggering and variability in heart rate. Recently, the first steps have been made towards clinical utility. Zun et al (93) performed myocardial rest and stress ASL in patients with and without ischemia based on first-pass perfusion MRI and X-ray coronary angiography. In patients without ischemia, myocardial ASL was capable of detecting clinically significant increases in myocardial blood flow after adenosine stress compared to rest. In the ischemic patients, myocardial perfusion reserve was found to be decreased in the most remote ischemic segments compared to healthy myocardium. For diagnosis of ischemia in the individual patient, however, several complex technical issues remain to be resolved, including the insufficient SNR at rest when myocardial blood flow is low.

DIFFUSION MRI. Cardiac diffusion tensor imaging (DTI) is a contrast-free technique that allows assessment of myocardial fiber structure in healthy and infarcted myocardium (94). Commonly, cardiac DTI is performed with up to 16 diffusion-encoding direction. To increase SNR, several acquisitions are averaged after spatiotemporal registration. The helix angle is used as a measure of myocardial fiber organization, which is defined as the inclination of the myocardial fibers out of the local radial plane. Whereas in the normal heart, the fiber architecture is highly coherent, infarction results in severe fiber disarrangement with high anisotropy. Chronic infarction is characterized by substantial loss of myocardial fibers in the infarct zone and a network of residual fibers propagating from border to core zone. In contrast to DTI of the brain, DTI of the heart is still limited to the research setting, due to technical challenges (including cardiac and respiratory motion, short myocardial T2, and magnetic field inhomogeneity) and long acquisition times (free-breathing whole-heart DTI is in the range of 15 minutes) (95).

CLINICAL INDICATIONS

Myocardial infarction

LATE GADOLINIUM ENHANCEMENT. LGE can be used to identify the location and the extent of irreversible injury of both acute and chronic myocardial infarction, with high accuracy and reproducibility (25). There is a close link in spatial delineation by LGE on cardiac MRI and myocardial necrosis or collagenous scar on histology, confirmed at various timepoints after infarction. LGE is capable of the detection of small subendocardial infarcts, given the high spatial resolution, which, in contrast to transmural infarcts, are systematically missed by single photon emission computed tomography (SPECT) (96,97). In patients with myocardial infarction, the extent of scarring as identified by LGE is a strong predictor for all-cause mortality and cardiac death (98). Likewise, in patients with known or suspected coronary artery disease, but without known prior myocardial infarction, the presence of LGE is a strong predictor of major adverse cardiovascular endpoints, even when taking into account the traditional clinical, angiographic, and functional variables, including the LV ejection fraction (99). Furthermore, studies confirmed an inverse relation between LGE transmurality and contractile response to pharmacological stress (100). In general, segments with less than 50% transmurality can be considered viable, and more than 10 viable segments indicate a high likelihood of recovery of cardiac function after revascularization (101). A reduction in the extent of LGE early after infarction can be interpreted as an early restoration of blood flow and is associated with functional improvement (102). In contrast, LGE in the infarct zone shortly after revascularization is an independent predictor of impaired LV systolic thickening and remodeling (103).

When performing LGE imaging after reperfusion therapy, there may be areas with lack of contrast within the hyperenhanced areas ("no-reflow" phenomenon) (**Figure 9**). This

observation has been explained as microvascular obstruction. Due to strong, prolonged impairment of myocardial perfusion as a result of microthrombi and swelling of ischemic tissue, contrast wash-in becomes severely impaired (104). More recently, however, evidence has been found that the hypoenhanced areas within the infarct core are not related to microvascular obstruction, but to severe microvascular injury and intramyocardial hemorrhage. Histologic assessment of an in vivo porcine model of reperfused ST-segment-elevation myocardial infarction (STEMI) showed in the hypointense areas severe disruption of the endothelial cells with extravasated erythrocytes, whereas the areas surrounding the infarct core showed an intact microvasculature with microthrombi (the true anatomical location of microvascular obstruction) (105). In view of above findings, studies have been performed on the prognostic value of intramyocardial hemorrhage, as assessed on T2 and T2* maps, in reperfused STEMI. Intramyocardial hemorrhage showed a closer association with adverse outcome, compared to microvascular obstruction, as assessed on LGE images (106).

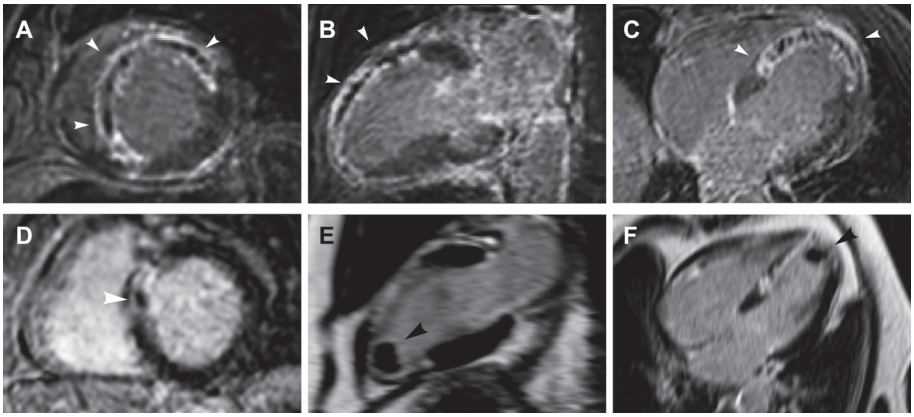

Figure 9. Example of 2D late gadolinium enhancement (LGE) images showing hypoenhanced areas in acute myocardial infarction after reperfusion therapy (white arrows). (**A–C**) an 81-year-old man, with a recent anteroseptal myocardial infarction and stenting of the left anterior descending (LAD) coronary artery. (**D–F**) a 65-year-old man, with a recent anteroseptal infarction and balloon dilating of the LAD. Note the thrombus formation in left ventricular apex (black arrows).

In the research setting, several other LGE-based variables have been studied that may have potential for clinical use. For instance, core and border zone characteristics may have potential for risk stratification for mortality in postinfarction patients (107). Border zone (peri-infarct zone) refers to areas with "intermediate" LGE intensity. Those regions consist of a mixture of healthy and diseased myocytes, which may represent a substrate for ventricular arrhythmia (108). Several definitions exist; for instance, the regions with an LGE intensity level between 2 to 3 standard deviations above the reference remote myocardial region or those with a signal intensity between 35–50% of the maximum in the infarct core. Another more advanced application, requiring high expert knowledge, is scar identification in the right ventricle (RV) and in the thin walls of the atria. Furthermore, recent work shows promise for early gadolinium enhancement for the detection of the areas at risk, marking both the reversibly and irreversibly injured myocardium based on an increase in extracellular volume (109). In contrast, conventional LGE provides information on the extent of infarcted myocardium, but does not provide information on the characteristics of viable myocardium; for instance, how well it will adapt to the increased work load and whether it is at risk for additional scarring.

NATIVE T1 MAPPING AND EXTRACELLULAR VOLUME MAPPING. Native T1 mapping may provide comparative information as the established LGE technique (110). Both acute and chronic myocardial infarcts may be identified on native T1 maps, as a result of edema and replacement fibrosis, respectively, with infarcts having higher native T1 relaxation times. Furthermore, when using native and postcontrast T1 mapping, acute and chronic infarcts may be differentiated on the basis of different patterns of contrast-induced T1 shortening. Possibly, this is due to a significant increase in distribution volume in acute necrosis and a smaller expansion of extracellular space in the chronic stage with scarring (111). ECV mapping has been shown to be significantly different in infarct tissue (51 ± 8%) compared to normal myocardium (27 ± 3%). A potential advantage, compared to conventional LGE images, is the additional information, beyond the binary information provided by LGE. ECV mapping has been shown to have potential for tracing subclinical abnormalities in non-LGE myocardium remote from infarcted areas (112).

A drawback is that native T1 and ECV mapping for ischemic cardiomyopathy is not that robust and artifact-free yet, as compared to LGE, and it seems difficult to determine the threshold values for abnormal and normal native T1 and ECV. Also, T1 mapping needs to be performed with sufficient spatial resolution to determine the infarct's transmurality.

Myocardial ischemia

STRESS PERFUSION AND STRESS WALL MOTION IMAGING. Current guidelines consider ischemia testing by cardiac MRI appropriate in patients with an intermediate likelihood of obstructive coronary artery disease, in patients with resting ECG abnormalities,

an uninterpretable ECG, or those incapable of exercise for stress ECG. High-risk patients should undergo invasive angiography directly (101). Cardiac MR stress perfusion imaging shows superior results compared to SPECT for the diagnosis of ischemia (113,114) and for the prediction of major adverse cardiac events (115). A meta-analysis on the diagnostic value of cardiac MR stress perfusion imaging for coronary artery disease showed, per-patient level, a sensitivity and specificity of 91% and 81%, respectively (116). A meta-analysis of dobutamine-stress wall motion cardiac MRI showed a sensitivity of 83% and specificity of 86% for the detection of coronary artery disease on a per-patient level (116). Also, dobutamine-stress wall motion in patients with resting akinetic wall segments can identify those who will improve in systolic function after revascularization (117,118). Regarding the prognostic value of abnormal adenosine-stress perfusion and dobutamine/atropine-stress wall motion, a 3-year event-free survival of 83.5% was reported, compared to 99.2% in patients with known or suspected coronary artery disease but with normal stress perfusion and stress wall motion imaging (119).

There is one study comparing both adenosine-stress perfusion and dobutamine/atropine wall motion imaging to invasive coronary angiography. Dobutamine-stress wall motion was superior to adenosine-stress perfusion, based on superior specificity (80% compared to 62%) (as it detects only patients with high-grade perfusion deficits) and comparable sensitivity (89% compared to 91%) (120). Most of the evidence regarding the diagnostic accuracy of stress perfusion and stress wall motion imaging is in individual studies, with various combinations in the studied image modality and stress agent, in different patient populations. Whether stress wall motion or stress perfusion imaging is preferable in under debate, and it is recommended that the method be used in which there is local expertise (53). Since stress imaging myocardium is typically combined with a LGE module, the patient will receive contrast material during the MR examination, even if stress wall motion imaging is chosen over stress perfusion imaging. If contrast material has already been administered for perfusion imaging (for example, 0.05 mmol/lg for stress and rest perfusion), an additional dose is given, to come to a total dose of 0.1–0.2 mmol/kg for LGE imaging (24).

NATIVE T1 MAPPING. Recently, there have been studies that may suggest that ischemia detection may be possible without contrast administration. Liu et al (121) showed that native T1 remains unchanged in infarcted tissue in response to adenosine stress, while there is an increase in native T1 in healthy tissue because of vasodilation (**Figure 10**). The principle lies in native T1 as a measure of myocardial blood volume and myocardial water content. The authors were able to distinguish normal, infarcted, ischemic, and remote myocardium, based on T1 mapping during adenosine vasodilatory stress and rest.

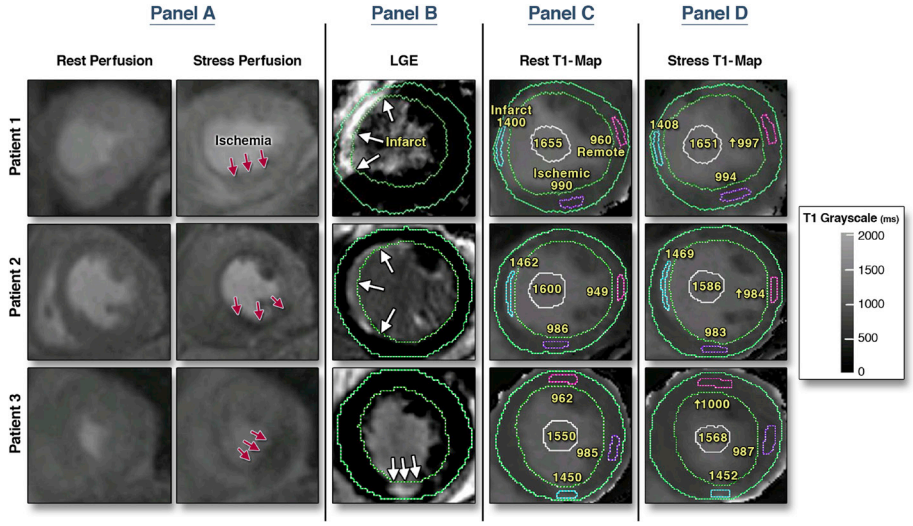

Figure 10. Example of noncontrast-enhanced myocardial perfusion based on native T1 measurements at rest and during adeno-sine stress. Ischemic areas can be identified on stress T1 mapping based on nonsignificant T1 reactivity, related to the absence of increased myocardial blood volume. Reprinted from Liu et al (121) under the terms of the Creative Commons Licence.

Nonischemic cardiomyopathy

LATE GADOLINIUM ENHANCEMENT. Although LGE is primarily performed in the context of ischemic heart disease, it is of significant clinical value in nonischemic cardiomyopathy as well. The different types of cardiomyopathy show typically different LGE patterns (**Figure 11**) (122). Ischemic cardiomyopathy is characterized by subendocardial and/or transmural LGE, whereas isolated midwall or subepicardial enhancement, not corresponding to any known coronary perfusion territory, is suggestive of nonischemic cardiomyopathy (123). For hypertrophic cardiomyopathy (HCM), LGE is seen at the junctions of the septum and RV free wall and in severely hypertrophic areas (124), most likely related to disorganized myocardial tissue and/or demand ischemia. For dilated cardiomyopathy (DCM), a typical finding is LGE midwall enhancement (125). Comparable to ischemic heart disease, the presence of LGE in HCM (126) and DCM (127) has strong predictive value for adverse cardiac events. Furthermore, amyloidosis (128) and sarcoidosis (129) can be identified based on diffuse subendocardial enhancement and more focal enhancement, respectively. In myocarditis, LGE can be observed in the lateral free wall (midwall and subepicardal enhancement) (130). LGE in the RV is typical for arrhythmogenic RV cardiomyopathy (ARVC) (131) and in Chagas disease (132).

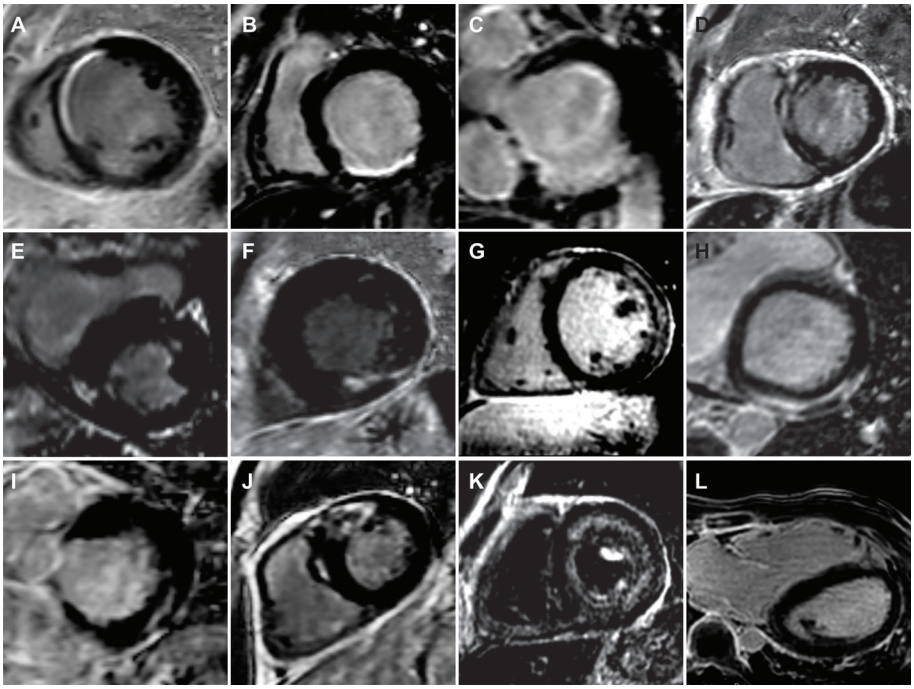

Figure 11. Examples of typical patterns of late gadolinium enhancement (LGE) in ischemic and nonischemic cardiomyopathy (A– K: 2D short-axis LGE images; L: 2D transverse LGE image). (**A**) Chronic subendocardial anteroseptal infarction, related to occlusion of the left anterior descending (LAD) coronary artery. (**B**) Chronic subendocardial inferior infarction, due to an occluded right coro-nary artery (RCA). (**C**) Transmural inferior infarction. (**D**) Dilated cardiomyopathy (DCM) with midwall LGE. (**E,F**) Hypertrophic car-diomyopathy (HCM) with typical LGE at the insertion points of the right ventricle (E) or in the hypertrophic areas (F). (**G,H**) Myocarditis with midwall (G) or subendocardial (H) LGE in the lateral free wall. (**I,J**) Sarcoidosis with typical focal LGE. (**K**) Amyloidosis with typical diffuse subendocardial LGE. (**L**) Arrhythmogenic right ventricular cardiomyopathy (ARVC), with typical LGE in the right ventricle.

NATIVE T1 MAPPING AND EXTRACELLULAR VOLUME MAPPING. Native T1 values have been shown to be increased in diffuse myocardial fibrosis in various nonischemic cardiomyopathies and amyloidosis, and reduced by lipid infiltration (Anderson-Fabry disease) or iron overload compared to normal myocardium (133). Interesting proof of native T1 mapping as an alternative to conventional contrast-based imaging protocols is the evaluation of acute myocarditis. While the standard criteria for diagnosis include early and late gadolinium enhancement criteria, Luetkens et al (134) showed that native T1 mapping even has superior diagnostic performance. Based on cellular edema, myocyte necrosis, and increased extracellular space, the T1 relaxation time is significantly prolonged in acute myocarditis.

A unique feature of ECV mapping, contrary to LGE, is the ability to detect diffuse changes in myocardial tissue. The technique is not dependent on spatial variation in fibrosis across the myocardium and does not need normal tissue as an internal reference. Edema, fibrosis, or amyloid, etc., result in an increase in ECV values. Several studies showed a correlation between ECV measured by cardiac MRI and histology (135). ECV has been associated with adverse outcome, in some cohorts even outperforming LV ejection fraction (136), and can therefore be regarded as an intrinsic myocardial characteristic.

Cardiac masses (including thrombus)

Using cardiac MRI, location, functional characteristics, and tissue composition of a cardiac mass can be evaluated, to dis-criminate benign and malignant tumors and to differentiate cardiac tumor from intracardiac thrombus (137). A typical MR examination for cardiac mass consists of T1-weighted FSE images for assessment of location and size, a T2-weighted FSE sequence with fat suppression for evaluation of edema and fibrosis within the cardiac mass, followed by first-pass perfusion imaging, postcontrast T1-weighted FSE with fat suppression, and LGE imaging (24). Based on the absence of contrast uptake, nonvascularized thrombus can be differentiated from tumor. Postcontrast serial imaging will help to differentiate a hypoperfused necrotic core from thrombus.

Lipoma can be recognized by low signal intensity on T2-weighted images, a dropout in signal intensity on T1-weighted images when using fat saturation, and no delayed enhancement. Myxoma and fibroma can be distinguished by high versus low T2-weighted signal and heterogeneous versus intense delayed enhancement, respectively. In general, malignant tumors have an irregular and invasive border and are of considerable size. Location in the right atrial wall or presence of pericardial effusion is suspicious for malignancy. Myxomas and fibromas may contain small calcifications, whereas large calcified foci are typical for osteosarcoma (137). A recent study showed the potential of T1 and T2 mapping to provide discriminative diagnostic information as an alternative to conventional T1-and T2-weighted images combined with LGE imaging (for example, for the diagnosis of papillary fibroelastomas) (138).

Coronary arteries

Coronary MRA (with or without contrast material) is considered appropriate for identifying coronary artery anomalies and aneurysm and for determining coronary artery patency, but is not appropriate for the detection of single-vessel disease (101). The first multicenter study on the diagnostic performance of coronary MRA for coronary artery disease was published by Kim et al in 2001 (139). The authors showed high specificity for the detection of left main coronary or three-vessel disease (100%), but insufficient sensitivity (85%) for ruling out coronary artery disease. They used a contrast-free GRE sequence, with a target volume approach consisting of repeated acquisitions of 3D double-oblique 3 cm volumes along the coronary arteries, with an

average scanning time of 70 minutes. Despite technical improvements in coronary MRA since then (140), and despite the insusceptibility to calcification in contrast to the blooming artifacts on CTA (141), the limited spatial resolution and long acquisition time render MR still inferior to CT for the assessment of coronary stenosis (142).

There are few studies comparing the diagnostic performance of coronary MRA with and without contrast material. A comparison between 3T GRE coronary MRA with slow infusion of contrast material and 1.5T noncontrast balanced SSFP coronary MRA in healthy volunteers resulted in higher CNR and superior visualization of the coronary segments for the contrast-enhanced compared to the noncontrast approach (143). Several studies compared image quality when using an extracellular or intravascular gadolinium chelate for coronary MRA. The intravascular agent gadofosveset trisodium shows slightly better or comparable performance (33,63,144).

Large vessels

Studies showed agreement in measured aortic diameter between contrast-enhanced MRA and unenhanced 3D balanced SSFP and equal sensitivity and specificity for the diagnosis of thoracic aorta pathologies (145). 3D balanced SSFP shows even better visualization of the aortic root and higher SNR and CNR for all segments (146). For peripheral MRA, contrast-enhanced MRA, compared to ECG-gated 3D partial-Fourier FSE, is superior in terms of robustness (fewer artifacts) and diagnostic accuracy for detection of stenosis (147,148).

For the evaluation of pulmonary veins pre-and postablation for atrial fibrillation (**Figure 6**), both contrast-enhanced MRA and noncontrast balanced SSFP have been proven to be accurate regarding detection of anatomic variants and measurement of pulmonary vein diameters (149). As signal void artifacts may occur due to off-resonance effects in non-contrast pulmonary vein imaging (150) and because the clinical MRI exam pre-and postablation typically includes LGE imaging for the evaluation of myocardial scar, in general, contrast-enhanced pulmonary vein MRA is used in clinical practice (24).

CONCLUSION

Contrast material in cardiac MRI should be used for tissue characterization in ischemic and nonischemic cardiomyopathy and may be used for stress perfusion imaging for the detection of ischemia. In cardiac-related vascular MRI, use of contrast material should be avoided, unless high-quality angiography is required that cannot be obtained with non-contrast protocols.

In general, noncontrast protocols should be preferred over contrast-enhanced techniques if the diagnostic performance is comparable. In all patients, dosage should be as low as possible. Differences between the available contrast agents in terms of chemical stability, relaxivity, and intravascular residence time may guide the choice of contrast agent. Gadolinium-

based contrast material in cardiac MRI should be avoided in patients with previous severe hypersensitivity reactions. Specific guidelines are available for the use of contrast material in patients with reduced renal function, in pregnant or lactating women, and in children. In patients at risk of impaired renal function, renal function should always be tested.

Cardiac structure and function is assessed by balanced SSFP cine imaging. Balanced SSFP generates an intrinsic high contrast between blood and myocardium based on the differences in the T2/T1 ratio. Velocity of flow across the valves can be measured using phase-contrast techniques. LGE imaging for myocardial scar visualization has been thoroughly validated in histological studies and the prognostic value of LGE has been confirmed in a variety of patient groups, in both acute and chronic stages of myocardial infarction and in nonischemic cardiomyopathy. Stress testing for ischemia can be performed with contrast-based first-pass imaging or contrast-free wall motion imaging. The choice of technique should depend on the local expertise available. Contrast-free native T1 mapping and contrast-based ECV mapping show promise for the evaluation of ischemic and nonischemic cardiomyopathy and may even provide additional information over conventional LGE imaging. However, prospective studies, against the standard of care, are needed to show whether these techniques represent alternatives to the current cardiac MR protocols in clinical routine. Contrast-enhanced and noncontrast MRA protocols are avail-able for the visualization of the coronary arteries and large vessels. For atherosclerotic plaque characterization in a research setting, contrast material can be of additive value.

In conclusion, the majority of cardiac MRI examinations rely on gadolinium-based contrast material, but a range of exciting noncontrast alternatives with high potential for clinical application are under development.

REFERENCES

1. Bruder O, Wagner A, Lombardi M, et al. European Cardiovascular Magnetic Resonance (EuroCMR) registry--multinational results from 57 centers in 15 countries. J Cardiovasc Magn Reson 2013;15:9.
2. American College of Radiology. ACR Manual on Contrast Media version 10.2 2016; https://www.acr.org/Quality-Safety/Resources/Contrast-Manual. Last accessed April 3, 2017.
3. European Society of Urogenital Radiology. ESUR Guidelines on Contrast Media 2012; http://www.esur.org/guidelines. Last accessed April 3, 2017.
4. U.S. Food and Drug Administration. Information for Healthcare Professionals: Gadolinium-Based Contrast Agents for Magnetic Resonance Imaging 2007; https://www.fda.gov/Drugs/DrugSafety/PostmarketDrugSafetyInformationforPatientsandProviders/ucm142884.htm. Last accessed April 3, 2017.
5. European Medicines Agency. Assessment report for Gadolinium-containing contrast agents 2010; http://www.ema.europa.eu/docs/en_GB/document_library/ Referrals_document/gadolinium_31/WC500099538.pdf. Last accessed April 3, 2017.
6. Reimer P, Vosshenrich R. Off-label use of contrast agents. Eur Radiol 2008;18:1096–1101.
7. U.S. Food and Drug Administration. "Off-label" and investigational use of marketed drugs, biologics and medical devices 2016; http://www.fda.gov/Regulatory Information/Guidances/ucm126486.htm. Last accessed December 1, 2016.
8. Wittich CM, Burkle CM, Lanier WL. Ten common questions (and their answers) about off-label drug use. Mayo Clin Proc 2012;87:982–990.
9. Prince MR, Zhang H, Zou Z, Staron RB, Brill PW. Incidence of Immediate Gadolinium Contrast Media Reactions. Am J Roentgenol 2011;196:W138–W143.
10. Bruder O, Schneider S, Pilz G, et al. 2015 Update on Acute Adverse Reactions to Gadolinium based Contrast Agents in Cardiovascular MR. Large Multi-National and Multi-Ethnical Population Experience With 37788 Patients From the EuroCMR Registry. J Cardiovasc Magn Reson 2015;17:58.
11. Jung J-W, Kang H-R, Kim M-H, et al. Immediate Hypersensitivity Reaction to Gadolinium-based MR Contrast Media. Radiology 2012;264:414–422.
12. Granata V, Cascella M, Fusco R, et al. Immediate Adverse Reactions to Gadolinium-Based MR Contrast Media: A Retrospective Analysis on 10,608 Examinations. Biomed Res Int 2016;2016:1–6.
13. Cowper SE, Robin HS, Steinberg SM, Su LD, Gupta S, LeBoit PE. Scleromyxoedema-like cutaneous diseases in renal-dialysis patients. Lancet 2000;356:1000–1001.
14. Todd DJ, Kay J. Gadolinium-Induced Fibrosis. Annu Rev Med 2016;67:273–291.
15. Prince MR, Zhang HL, Prowda JC, Grossman ME, Silvers DN. Nephrogenic systemic fibrosis and its impact on abdominal imaging. Radiographics 2009;29:1565–1574.
16. Reiter T, Ritter O, Prince MR, et al. Minimizing Risk of Nephrogenic systemic fibrosis in Cardiovascular Magnetic Resonance. J Cardiovasc Magn Reson 2012;14:31.
17. Kanda T, Ishii K, Kawaguchi H, Kitajima K, Takenaka D. High signal intensity in the dentate nucleus and globus pallidus on unenhanced T1-weighted MR images: relationship with increasing cumulative dose of a gadolinium-based contrast material. Radiology 2014;270:834–841.
18. Kanda T, Fukusato T, Matsuda M, et al. Gadolinium-based Contrast Agent Accumulates in the Brain Even in Subjects without Severe Renal Dysfunction: Evaluation of Autopsy Brain Specimens with Inductively Coupled Plasma Mass Spectroscopy. Radiology 2015;276:228–232.
19. McDonald RJ, McDonald JS, Kallmes DF, et al. Intracranial Gadolinium Deposition after Contrast-enhanced MR Imaging. Radiology 2015;275:772–782.
20. Radbruch A. Are some agents less likely to deposit gadolinium in the brain? Magn Reson Imaging 2016;34:1351–1354.
21. U.S. Food and Drug Administration. FDA Drug Safety Communication: New warnings for using gadolinium-based contrast agents in patients with kidney dysfunction 2010; https://www.fda.gov/Drugs/DrugSafety/ucm223966.htm. Last accessed April 3, 2017.
22. Fraum TJ, Ludwig DR, Bashir MR, Fowler KJ. Gadolinium-based contrast agents: A comprehensive risk assessment. J Magn Reson Imaging 2017;
23. Nacif MS, Arai AE, Lima JAC, Bluemke D. Gadolinium-enhanced cardiovascular

magnetic resonance: administered dose in relationship to United States Food and Drug Administration (FDA) guidelines. J Cardiovasc Magn Reson 2012;14:18.
24. Kramer CM, Barkhausen J, Flamm SD, Kim RJ, Nagel E. Standardized cardiovascular magnetic resonance (CMR) protocols 2013 update. J Cardiovasc Magn Reson 2013;15:91.
25. Kim RJ, Albert TSE, Wible JH, et al. Performance of Delayed-Enhancement Magnetic Resonance Imaging With Gadoversetamide Contrast for the Detection and Assessment of Myocardial Infarction: An International, Multicenter, Double-Blinded, Randomized Trial. Circulation 2008;117:629–637.
26. Wolff SD, Schwitter J, Coulden R, et al. Myocardial first-pass perfusion magnetic resonance imaging: a multicenter dose-ranging study. Circulation 2004;110:732–737.
27. Giang TH, Nanz D, Coulden R, et al. Detection of coronary artery disease by magnetic resonance myocardial perfusion imaging with various contrast medium doses: First european multi-centre experience. Eur Heart J 2004;25:1657–1665.
28. Gibby WA. MRI contrast agents. Zimmerman RA, Gibby WA, Carmody RF, editors. In: Neuroimaging: Clinical and Physical Principles. New York: Springer; 2000. p 313–364.
29. Port M, Idée J-M, Medina C, Robic C, Sabatou M, Corot C. Efficiency, thermodynamic and kinetic stability of marketed gadolinium chelates and their possible clinical consequences: a critical review. BioMetals 2008;21:469–490.
30. Lohrke J, Frenzel T, Endrikat J, et al. 25 Years of Contrast-Enhanced MRI: Developments, Current Challenges and Future Perspectives. Adv Ther 2016;33:1–28.
31. Wildgruber M, Stadlbauer T, Rasper M, et al. Single-Dose Gadobutrol in Comparison With Single-Dose Gadobenate Dimeglumine for Magnetic Resonance Imaging of Chronic Myocardial Infarction at 3 T. Invest Radiol 2014;49:728–734.
32. Hartmann M, Wiethoff AJ, Hentrich H-R, Rohrer M. Initial imaging recommendations for Vasovist angiography. Eur Radiol 2006;16 Suppl 2:B15-23.
33. Raman FS, Nacif MS, Cater G, et al. 3.0-T whole-heart coronary magnetic resonance angiography: comparison of gadobenate dimeglumine and gadofosveset trisodium. Int J Cardiovasc Imaging 2013;29:1085–1094.
34. Li W, Tutton S, Vu AT, et al. First-pass contrast-enhanced magnetic resonance angiography in humans using ferumoxytol, a novel ultrasmall superparamagnetic iron oxide (USPIO)-based blood pool agent. J Magn Reson Imaging 2005;21:46–52.
35. Hope MD, Hope TA, Zhu C, et al. Vascular Imaging With Ferumoxytol as a Contrast Agent. Am J Roentgenol 2015;205:W366–W373.
36. Finn JP, Nguyen K-L, Han F, et al. Cardiovascular MRI with ferumoxytol. Clin Radiol 2016;71:796–806.
37. Schiller B, Bhat P, Sharma A. Safety and Effectiveness of Ferumoxytol in Hemodialysis Patients at 3 Dialysis Chains in the United States Over a 12-Month Period. Clin Ther 2014;36:70–83.
38. Nguyen K-L, Yoshida T, Han F, et al. MRI with ferumoxytol: A single center experience of safety across the age spectrum. J Magn Reson Imaging 2017;45:804–812.
39. Thiele H, Nagel E, Paetsch I, et al. Functional cardiac MR imaging with steady-state free precession (SSFP) significantly improves endocardial border delineation without contrast agents. J Magn Reson Imaging 2001;14:362–367.
40. Dyverfeldt P, Bissell M, Barker AJ, et al. 4D flow cardiovascular magnetic resonance consensus statement. J Cardiovasc Magn Reson 2015;17:72.
41. Kim RJ, Chen E-L, Lima JAC, Judd RM. Myocardial Gd-DTPA Kinetics Determine MRI Contrast Enhancement and Reflect the Extent and Severity of Myocardial Injury After Acute Reperfused Infarction. Circulation 1996;94:3318–3326.
42. Young IR, Bailes DR, Bydder GM. Apparent changes of appearance of inversion-recovery images. Magn Reson Med 1985;2:81–85.
43. Noll DC, Nishimura DG, Macovski A. Homodyne detection in magnetic resonance imaging. IEEE Trans Med Imaging 1991;10:154–163.
44. Kellman P, Arai AE, McVeigh ER, Aletras AH. Phase-sensitive inversion recovery for detecting myocardial infarction using gadolinium-delayed hyperenhancement. Magn Reson Med 2002;47:372–383.
45. Bizino M, Amersfoort J, Tao Q, van der Geest RJ, Lamb HJ. Free-breathing 3D phase-sensitive inversion recovery late gadolinium enhancement at 3.0 Tesla: reliability and image quality in ischemic and non-ischemic cardiomyopathy in comparison with multiple breath-hold 3D imaging. J Cardiovasc Magn Reson 2015;17:P97.
46. Piehler KM, Wong TC, Puntil KS, et al. Free-

Breathing, Motion-Corrected Late Gadolinium Enhancement Is Robust and Extends Risk Stratification to Vulnerable Patients. Circ Cardiovasc Imaging 2013;6:423–432.
47. Varga-Szemes A, van der Geest RJ, Spottiswoode BS, et al. Myocardial Late Gadolinium Enhancement: Accuracy of T1 Mapping–based Synthetic Inversion-Recovery Imaging. Radiology 2016;278:374–382.
48. Gould KL, Lipscomb K. Effects of coronary stenoses on coronary flow reserve and resistance. Am J Cardiol 1974;34:48–55.
49. Rieber J. Cardiac magnetic resonance perfusion imaging for the functional assessment of coronary artery disease: a comparison with coronary angiography and fractional flow reserve. Eur Heart J 2005;27:1465–1471.
50. Al-Saadi N, Nagel E, Gross M, et al. Noninvasive Detection of Myocardial Ischemia From Perfusion Reserve Based on Cardiovascular Magnetic Resonance. Circulation 2000;101:1379–1383.
51. Schaefer S, Tyen R Van, Saloner D. Evaluation of myocardial perfusion abnormalities with gadolinium-enhanced snapshot MR imaging in humans. Work in progress. Radiology 1992;185:795.
52. Baer FM, Voth E, Theissen P, Schicha H, Sechtem U. Gradient-echo magnetic resonance imaging during incremental dobutamine infusion for the localization of coronary artery stenoses. Eur Heart J 1994;15:218–225.
53. Nagel E. Moving Toward the Optimal Test for the Assessment of Myocardial Ischemia. J Am Heart Assoc 2016;5:e003266.
54. Taylor AJ, Salerno M, Dharmakumar R, Jerosch-Herold M. T1 Mapping. JACC Cardiovasc Imaging 2016;9:67–81.
55. Treibel TA, Fontana M, Maestrini V, et al. Automatic Measurement of the Myocardial Interstitium. JACC Cardiovasc Imaging 2016;9:54–63.
56. Kawel N, Nacif M, Zavodni A, et al. T1 mapping of the myocardium: Intra-individual assessment of the effect of field strength, cardiac cycle and variation by myocardial region. J Cardiovasc Magn Reson 2012;14:27.
57. Higgins DM, Moon JC. Review of T1 Mapping Methods: Comparative Effectiveness Including Reproducibility Issues. Curr Cardiovasc Imaging Rep 2014;7:9252.
58. Captur G, Manisty C, Moon JC. Cardiac MRI evaluation of myocardial disease. Heart 2016;102:1429–1435.
59. Moon JC, Messroghli DR, Kellman P, et al. Myocardial T1 mapping and extracellular volume quantification: a Society for Cardiovascular Magnetic Resonance (SCMR) and CMR Working Group of the European Society of Cardiology consensus statement. J Cardiovasc Magn Reson 2013;15:92.
60. Dabir D, Child N, Kalra A, et al. Reference values for healthy human myocardium using a T1 mapping methodology: results from the International T1 Multicenter cardiovascular magnetic resonance study. J Cardiovasc Magn Reson 2014;16:69.
61. Bi X, Carr JC, Li D. Whole-heart coronary magnetic resonance angiography at 3 Tesla in 5 minutes with slow infusion of Gd-BOPTA, a high-relaxivity clinical contrast agent. Magn Reson Med 2007;58:1–7.
62. Yang Q, Li K, Liu X, et al. Contrast-Enhanced Whole-Heart Coronary Magnetic Resonance Angiography at 3.0-T. A Comparative Study With X-Ray Angiography in a Single Center. J Am Coll Cardiol 2009;54:69–76.
63. Wagner M, Rösler R, Lembcke A, et al. Whole-Heart Coronary Magnetic Resonance Angiography at 1.5 Tesla: does a blood-pool contrast agent improve diagnostic accuracy? Invest Radiol 2011;46:152–159.
64. Maintz D, Aepfelbacher FC, Kissinger K V., et al. Coronary MR Angiography: Comparison of Quantitative and Qualitative Data from Four Techniques. Am J Roentgenol 2004;182:515–521.
65. Li D, Paschal CB, Haacke EM, Adler LP. Coronary arteries: three-dimensional MR imaging with fat saturation and magnetization transfer contrast. Radiology 1993;187:401–406.
66. Börnert P, Koken P, Nehrke K, Eggers H, Ostendorf P. Water/fat-resolved whole-heart Dixon coronary MRA: An initial comparison. Magn Reson Med 2014;71:156–163.
67. Fayad ZA, Fuster V, Fallon JT, et al. Noninvasive In Vivo Human Coronary Artery Lumen and Wall Imaging Using Black-Blood Magnetic Resonance Imaging. Circulation 2000;102:506–510.
68. Botnar RM, Kim WY, Börnert P, Stuber M, Spuentrup E, Manning WJ. 3D coronary vessel wall imaging utilizing a local inversion technique with spiral image acquisition. Magn Reson Med 2001;46:848–854.
69. Macedo R, Chen S, Lai S, et al. MRI detects increased coronary wall thickness in asymptomatic individuals: The multi-ethnic study of atherosclerosis (MESA). J Magn Reson Imaging 2008;28:1108–1115.

70. Kim WY, Stuber M, Börnert P, Kissinger K V, Manning WJ, Botnar RM. Three-dimensional black-blood cardiac magnetic resonance coronary vessel wall imaging detects positive arterial remodeling in patients with nonsignificant coronary artery disease. Circulation 2002;106:296–299.
71. Kerwin WS, O'Brien KD, Ferguson MS, Polissar N, Hatsukami TS, Yuan C. Inflammation in carotid atherosclerotic plaque: a dynamic contrast-enhanced MR imaging study. Radiology 2006;241:459–468.
72. Wasserman BA, Smith WI, Trout HH, Cannon RO, Balaban RS, Arai AE. Carotid artery atherosclerosis: in vivo morphologic characterization with gadolinium-enhanced double-oblique MR imaging initial results. Radiology 2002;223:566–573.
73. Maintz D, Ozgun M, Hoffmeier A, et al. Selective coronary artery plaque visualization and differentiation by contrast-enhanced inversion prepared MRI. Eur Heart J 2006;27:1732–1736.
74. Yeon SB, Sabir A, Clouse M, et al. Delayed-Enhancement Cardiovascular Magnetic Resonance Coronary Artery Wall Imaging. J Am Coll Cardiol 2007;50:441–447.
75. Ibrahim T, Makowski MR, Jankauskas A, et al. Serial Contrast-Enhanced Cardiac Magnetic Resonance Imaging Demonstrates Regression of Hyperenhancement Within the Coronary Artery Wall in Patients After Acute Myocardial Infarction. JACC Cardiovasc Imaging 2009;2:580–588.
76. Kooi ME, Cappendijk VC, Cleutjens KBJM, et al. Accumulation of ultrasmall superparamagnetic particles of iron oxide in human atherosclerotic plaques can be detected by in vivo magnetic resonance imaging. Circulation 2003;107:2453–2458.
77. Botnar RM, Buecker A, Wiethoff AJ, et al. In vivo magnetic resonance imaging of coronary thrombosis using a fibrin-binding molecular magnetic resonance contrast agent. Circulation 2004;110:1463–1466.
78. Makowski MR, Wiethoff AJ, Blume U, et al. Assessment of atherosclerotic plaque burden with an elastin-specific magnetic resonance contrast agent. Nat Med 2011;17:383–388.
79. Fayad ZA. MR imaging for the noninvasive assessment of atherothrombotic plaques. Magn Reson Imaging Clin N Am 2003;11:101–113.
80. Kawasaki T, Koga S, Koga N, et al. Characterization of Hyperintense Plaque With Noncontrast T1-Weighted Cardiac Magnetic Resonance Coronary Plaque Imaging. Comparison With Multislice Computed Tomography and Intravascular Ultrasound. JACC Cardiovasc Imaging 2009;2:720–728.
81. Noguchi T, Kawasaki T, Tanaka A, et al. High-Intensity Signals in Coronary Plaques on Noncontrast T1-Weighted Magnetic Resonance Imaging as a Novel Determinant of Coronary Events. J Am Coll Cardiol 2014;63:989–999.
82. Prince MR. Gadolinium-enhanced MR aortography. Radiology 1994;191:155–164.
83. Lohan DG, Saleh R, Nael K, Krishnam M, Finn JP. Contrast-enhanced MRA versus nonenhanced MRA: Pros and cons. Appl Radiol 2007;36:3–15.
84. Wheaton AJ, Miyazaki M. Non-contrast enhanced MR angiography: Physical principles. J Magn Reson Imaging 2012;36:286–304.
85. Miyazaki M, Lee VS. Nonenhanced MR Angiography. Radiology 2008;248:20–43.
86. Hartung MP, Grist TM, François CJ. Magnetic resonance angiography: current status and future directions. J Cardiovasc Magn Reson 2011;13:19.
87. Wedeen VJ, Meuli R a, Edelman RR, et al. Projective imaging of pulsatile flow with magnetic resonance. Science 1985;230:946–948.
88. Dumoulin CL, Souza SP, Walker MF, Wagle W. Three-dimensional phase contrast angiography. Magn Reson Med 1989;9:139–149.
89. Ståhlberg F, Søndergaard L, Thomsen C, Henriksen O. Quantification of complex flow using MR phase imaging—A study of parameters influencing the phase/velocity relation. Magn Reson Imaging 1992;10:13–23.
90. Edelman RR, Sheehan JJ, Dunkle E, Schindler N, Carr J, Koktzoglou I. Quiescent-interval single-shot unenhanced magnetic resonance angiography of peripheral vascular disease: Technical considerations and clinical feasibility. Magn Reson Med 2010;63:951–958.
91. Miyazaki M, Sugiura S, Tateishi F, Wada H, Kassai Y, Abe H. Non-contrast-enhanced MR angiography using 3D ECG-synchronized half-Fourier fast spin echo. J Magn Reson Imaging 2000;12:776–783.
92. Kober F, Jao T, Troalen T, Nayak KS. Myocardial arterial spin labeling. J Cardiovasc Magn Reson 2016;18:22.
93. Zun Z, Varadarajan P, Pai RG, Wong EC, Nayak KS. Arterial Spin Labeled CMR Detects Clinically Relevant Increase in Myocardial Blood Flow With Vasodilation. JACC Cardiovasc Imaging 2011;4:1253–1261.

94. Mekkaoui C, Reese TG, Jackowski MP, Bhat H, Sosnovik DE. Diffusion MRI in the heart. NMR Biomed 2017;30:e3426.
95. Mekkaoui C, Reese TG, Jackowski MP, et al. Diffusion Tractography of the Entire Left Ventricle by Using Free-breathing Accelerated Simultaneous Multisection Imaging. Radiology 2017;282:850–856.
96. Wagner A, Mahrholdt H, Holly TA, et al. Contrast-enhanced MRI and routine single photon emission computed tomography (SPECT) perfusion imaging for detection of subendocardial myocardial infarcts: an imaging study. Lancet 2003;361:374–379.
97. Ibrahim T, Bülow HP, Hackl T, et al. Diagnostic Value of Contrast-Enhanced Magnetic Resonance Imaging and Single-Photon Emission Computed Tomography for Detection of Myocardial Necrosis Early After Acute Myocardial Infarction. J Am Coll Cardiol 2007;49:208–216.
98. Lee S-A, Yoon YE, Kim J-E, et al. Long-Term Prognostic Value of Late Gadolinium-Enhanced Magnetic Resonance Imaging in Patients With and Without Left Ventricular Dysfunction Undergoing Coronary Artery Bypass Grafting. Am J Cardiol 2016;118:1647–1654.
99. Kwong RY. Impact of Unrecognized Myocardial Scar Detected by Cardiac Magnetic Resonance Imaging on Event-Free Survival in Patients Presenting With Signs or Symptoms of Coronary Artery Disease. Circulation 2006;113:2733–2743.
100. Gerber BL, Rochitte CE, Bluemke D a, et al. Relation Between Gd-DTPA Contrast Enhancement and Regional Inotropic Response in the Periphery and Center of Myocardial Infarction. Circulation 2001;104:998–1004.
101. Hundley WG, Bluemke DA, Finn JP, et al. ACCF/ACR/AHA/NASCI/SCMR 2010 expert consensus document on cardiovascular magnetic resonance: A report of the american college of cardiology foundation task force on expert consensus documents. Circulation 2010;121:2462–2508.
102. Hillenbrand HB, Kim RJ, Parker M a, Fieno DS, Judd RM. Early assessment of myocardial salvage by contrast-enhanced magnetic resonance imaging. Circulation 2000;102:1678–1683.
103. Baks T, van Geuns R-J, Biagini E, et al. Effects of primary angioplasty for acute myocardial infarction on early and late infarct size and left ventricular wall characteristics. J Am Coll Cardiol 2006;47:40–44.
104. van Kranenburg M, Magro M, Thiele H, et al. Prognostic Value of Microvascular Obstruction and Infarct Size, as Measured by CMR in STEMI Patients. JACC Cardiovasc Imaging 2014;7:930–939.
105. Robbers LFHJ, Eerenberg ES, Teunissen PFA, et al. Magnetic resonance imaging-defined areas of microvascular obstruction after acute myocardial infarction represent microvascular destruction and haemorrhage. Eur Heart J 2013;34:2346–2353.
106. Carrick D, Haig C, Ahmed N, et al. Myocardial Hemorrhage After Acute Reperfused ST-Segment-Elevation Myocardial Infarction: Relation to Microvascular Obstruction and Prognostic Significance. Circ Cardiovasc Imaging 2016;9:e004148.
107. Yan AT. Characterization of the Peri-Infarct Zone by Contrast-Enhanced Cardiac Magnetic Resonance Imaging Is a Powerful Predictor of Post-Myocardial Infarction Mortality. Circulation 2006;114:32–39.
108. Schmidt A, Azevedo CF, Cheng A, et al. Infarct Tissue Heterogeneity by Magnetic Resonance Imaging Identifies Enhanced Cardiac Arrhythmia Susceptibility in Patients With Left Ventricular Dysfunction. Circulation 2007;115:2006–2014.
109. Hammer-Hansen S, Leung SW, Hsu L-Y, et al. Early Gadolinium Enhancement for Determination of Area at Risk. JACC Cardiovasc Imaging 2017;10:130–139.
110. Nagel E, Puntmann VO. Is Myocardial Native T1 the One Answer for All? JACC Cardiovasc Imaging 2016;9:37–39.
111. Messroghli DR, Walters K, Plein S, et al. Myocardial T1 mapping: Application to patients with acute and chronic myocardial infarction. Magn Reson Med 2007;58:34–40.
112. Ugander M, Oki AJ, Hsu L-Y, et al. Extracellular volume imaging by magnetic resonance imaging provides insights into overt and sub-clinical myocardial pathology. Eur Heart J 2012;33:1268–1278.
113. Greenwood JP, Maredia N, Younger JF, et al. Cardiovascular magnetic resonance and single-photon emission computed tomography for diagnosis of coronary heart disease (CE-MARC): A prospective trial. Lancet 2012;379:453–460.
114. Schwitter J, Wacker CM, van Rossum AC, et al. MR-IMPACT: comparison of perfusion-cardiac magnetic resonance with single-photon emission computed tomography for the detection of coronary artery disease in a multicentre, multivendor, randomized trial. Eur

Heart J 2008;29:480–489.
115. Greenwood JP, Herzog BA, Brown JM, et al. Prognostic value of cardiovascular magnetic resonance and single-photon emission computed tomography in suspected coronary heart disease: Long-term follow-up of a prospective, diagnostic accuracy cohort study. Ann Intern Med 2016;165:1–9.
116. Nandalur KR, Dwamena BA, Choudhri AF, Nandalur MR, Carlos RC. Diagnostic Performance of Stress Cardiac Magnetic Resonance Imaging in the Detection of Coronary Artery Disease. J Am Coll Cardiol 2007;50:1343–1353.
117. Baer FM, Theissen P, Schneider CA, et al. Dobutamine Magnetic Resonance Imaging Predicts Contractile Recovery of Chronically Dysfunctional Myocardium After Successful Revascularization. J Am Coll Cardiol 1998;31:1040–1048.
118. Sayad DE, Willett DL, Hundley WG, Grayburn PA, Peshock RM. Dobutamine magnetic resonance imaging with myocardial tagging quantitatively predicts improvement in regional function after revascularization. Am J Cardiol 1998;82:1149–1151.
119. Jahnke C, Nagel E, Gebker R, et al. Prognostic value of cardiac magnetic resonance stress tests: Adenosine stress perfusion and dobutamine stress wall motion imaging. Circulation 2007;115:1769–1776.
120. Paetsch I, Jahnke C, Wahl A, et al. Comparison of dobutamine stress magnetic resonance, adenosine stress magnetic resonance, and adenosine stress magnetic resonance perfusion. Circulation 2004;110:835–842.
121. Liu A, Wijesurendra RS, Francis JM, et al. Adenosine Stress and Rest T1 Mapping Can Differentiate Between Ischemic, Infarcted, Remote, and Normal Myocardium Without the Need for Gadolinium Contrast Agents. JACC Cardiovasc Imaging 2016;9:27–36.
122. Cummings KW, Bhalla S, Javidan-Nejad C, Bierhals AJ, Gutierrez FR, Woodard PK. A pattern-based approach to assessment of delayed enhancement in nonischemic cardiomyopathy at MR imaging. Radiographics 2009;29:89–103.
123. Mahrholdt H, Wagner A, Judd RM, Sechtem U, Kim RJ. Delayed enhancement cardiovascular magnetic resonance assessment of non-ischaemic cardiomyopathies. Eur Heart J 2005;26:1461–1474.
124. Choudhury L, Mahrholdt H, Wagner A, et al. Myocardial scarring in asymptomatic or mildly symptomatic patients with hypertrophic cardiomyopathy. J Am Coll Cardiol 2002;40:2156–2164.
125. McCrohon JA, Moon JCC, Prasad SK, et al. Differentiation of heart failure related to dilated cardiomyopathy and coronary artery disease using gadolinium-enhanced cardiovascular magnetic resonance. Circulation 2003;108:54–59.
126. Chan RH, Maron BJ, Olivotto I, et al. Prognostic value of quantitative contrast-enhanced cardiovascular magnetic resonance for the evaluation of sudden death risk in patients with hypertrophic cardiomyopathy. Circulation 2014;130:484–495.
127. Assomull RG, Prasad SK, Lyne J, et al. Cardiovascular Magnetic Resonance, Fibrosis, and Prognosis in Dilated Cardiomyopathy. J Am Coll Cardiol 2006;48:1977–1985.
128. Maceira AM, Joshi J, Prasad SK, et al. Cardiovascular magnetic resonance in cardiac amyloidosis. Circulation 2005;111:186–193.
129. Smedema J-P, Snoep G, van Kroonenburgh MPG, et al. Evaluation of the accuracy of gadolinium-enhanced cardiovascular magnetic resonance in the diagnosis of cardiac sarcoidosis. J Am Coll Cardiol 2005;45:1683–1690.
130. Mahrholdt H. Cardiovascular Magnetic Resonance Assessment of Human Myocarditis: A Comparison to Histology and Molecular Pathology. Circulation 2004;109:1250–1258.
131. Tandri H, Saranathan M, Rodriguez ER, et al. Noninvasive detection of myocardial fibrosis in arrhythmogenic right ventricular cardiomyopathy using delayed-enhancement magnetic resonance imaging. J Am Coll Cardiol 2005;45:98–103.
132. Patel R, DiMarco J, Akar J, Voros S, Kramer C. Chagas Myocarditis and Syncope. J Cardiovasc Magn Reson 2005;7:685–688.
133. Puntmann VO, Peker E, Chandrashekhar Y, Nagel E. T1 Mapping in Characterizing Myocardial Disease. Circ Res 2016;119:277–299.
134. Luetkens JA, Homsi R, Sprinkart AM, et al. Incremental value of quantitative CMR including parametric mapping for the diagnosis of acute myocarditis. Eur Hear J – Cardiovasc Imaging 2016;17:154–161.
135. de Meester de Ravenstein C, Bouzin C, Lazam S, et al. Histological Validation of measurement of diffuse interstitial myocardial fibrosis by myocardial extravascular volume fraction from Modified Look-Locker imaging (MOLLI) T1 mapping at 3 T. J Cardiovasc Magn Reson

2015;17:48.
136. Schelbert EB, Piehler KM, Zareba KM, et al. Myocardial Fibrosis Quantified by Extracellular Volume Is Associated With Subsequent Hospitalization for Heart Failure, Death, or Both Across the Spectrum of Ejection Fraction and Heart Failure Stage. J Am Heart Assoc 2015;4:e002613.
137. O'Donnell DH, Abbara S, Chaithiraphan V, et al. Cardiac Tumors: Optimal Cardiac MR Sequences and Spectrum of Imaging Appearances. Am J Roentgenol 2009;193:377–387.
138. Caspar T, El Ghannudi S, Ohana M, et al. Magnetic resonance evaluation of cardiac thrombi and masses by T1 and T2 mapping: an observational study. Int J Cardiovasc Imaging 2016;
139. Kim WY, Danias PG, Stuber M, et al. Coronary magnetic resonance angiography for the detection of coronary stenoses. N Engl J Med 2001;345:1863–1869.
140. Yonezawa M, Nagata M, Kitagawa K, et al. Quantitative Analysis of 1.5-T Whole-Heart Coronary MR Angiograms Obtained with 32-Channel Cardiac Coils: A Comparison with Conventional Quantitative Coronary Angiography. Radiology 2014;271:356–364.
141. Liu X, Zhao X, Huang J, et al. Comparison of 3D Free-Breathing Coronary MR Angiography and 64-MDCT Angiography for Detection of Coronary Stenosis in Patients with High Calcium Scores. Am J Roentgenol 2007;189:1326–1332.
142. Schuetz GM, Zacharopoulou NM, Schlattmann P, Dewey M. Meta-analysis: Noninvasive Coronary Angiography Using Computed Tomography Versus Magnetic Resonance Imaging. Ann Intern Med 2010;125:167–177.
143. Liu X, Bi X, Huang J, Jerecic R, Carr J, Li D. Contrast-Enhanced Whole-Heart Coronary Magnetic Resonance Angiography at 3.0 T. Invest Radiol 2008;43:663–668.
144. Camren GP, Wilson GJ, Bamra VR, Nguyen KQ, Hippe DS, Maki JH. A Comparison between Gadofosveset Trisodium and Gadobenate Dimeglumine for Steady State MRA of the Thoracic Vasculature. Biomed Res Int 2014;2014:1–6.
145. François CJ, Tuite D, Deshpande V, Jerecic R, Weale P, Carr JC. Unenhanced MR angiography of the thoracic aorta: initial clinical evaluation. AJR Am J Roentgenol 2008;190:902–906.
146. Krishnam MS, Tomasian A, Malik S, Desphande V, Laub G, Ruehm SG. Image quality and diagnostic accuracy of unenhanced SSFP MR angiography compared with conventional contrast-enhanced MR angiography for the assessment of thoracic aortic diseases. Eur Radiol 2010;20:1311–1320.
147. Lim RP, Hecht EM, Xu J, et al. 3D nongadolinium-enhanced ECG-gated MRA of the distal lower extremities: Preliminary clinical experience. J Magn Reson Imaging 2008;28:181–189.
148. Haneder S, Attenberger UI, Riffel P, Henzler T, Schoenberg SO, Michaely HJ. Magnetic resonance angiography (MRA) of the calf station at 3.0 T: intraindividual comparison of non-enhanced ECG-gated flow-dependent MRA, continuous table movement MRA and time-resolved MRA. Eur Radiol 2011;21:1452–1461.
149. François CJ, Tuite D, Deshpande V, Jerecic R, Weale P, Carr JC. Pulmonary Vein Imaging with Unenhanced Three-dimensional Balanced Steady-State Free Precession MR Angiography: Initial Clinical Evaluation. Radiology 2009;250:932–939.
150. Hu P, Stoeck CT, Smink J, et al. Noncontrast SSFP pulmonary vein magnetic resonance angiography: Impact of off-resonance and flow. J Magn Reson Imaging 2010;32:1255–1261.